

FEB 6 1968

[REDACTED]

SC-PR-67-3023

January 1968

UNCLASSIFIED

MASTER

**AEROSPACE
NUCLEAR
SAFETY**



SANDIA LABORATORIES QUARTERLY REPORT
AEROSPACE NUCLEAR SAFETY PROGRAM
OCTOBER 1 TO DECEMBER 31, 1967

AEROSPACE NUCLEAR SAFETY DEPARTMENT 9310
SANDIA LABORATORY

[REDACTED]

DISTRIBUTION OF THIS DOCUMENT IS UNLIMITED

GROUPS excluded from automatic downgrading and declassification

68 9120

UNCLASSIFIED

SANDIA LABORATORIES



OPERATED FOR THE UNITED STATES ATOMIC ENERGY COMMISSION BY SANDIA CORPORATION | ALBUQUERQUE NEW MEXICO LIVERMORE CALIFORNIA

[REDACTED]

[REDACTED]

DISCLAIMER

This report was prepared as an account of work sponsored by an agency of the United States Government. Neither the United States Government nor any agency Thereof, nor any of their employees, makes any warranty, express or implied, or assumes any legal liability or responsibility for the accuracy, completeness, or usefulness of any information, apparatus, product, or process disclosed, or represents that its use would not infringe privately owned rights. Reference herein to any specific commercial product, process, or service by trade name, trademark, manufacturer, or otherwise does not necessarily constitute or imply its endorsement, recommendation, or favoring by the United States Government or any agency thereof. The views and opinions of authors expressed herein do not necessarily state or reflect those of the United States Government or any agency thereof.

DISCLAIMER

Portions of this document may be illegible in electronic image products. Images are produced from the best available original document.

[REDACTED]

Issued by Sandia Corporation,
a prime contractor to the
United States Atomic Energy Commission

LEGAL NOTICE

This report was prepared as an account of Government sponsored work. Neither the United States, nor the Commission, nor any person acting on behalf of the Commission:

A. Makes any warranty or representation, expressed or implied, with respect to the accuracy, completeness, or usefulness of the information contained in this report, or that the use of any information, apparatus, method, or process disclosed in this report may not infringe privately owned rights; or

B. Assumes any liabilities with respect to the use of, or for damages resulting from the use of any information, apparatus, method, or process disclosed in this report.

As used in the above, "person acting on behalf of the Commission" includes any employee or contractor of the Commission, or employee of such contractor, to the extent that such employee or contractor of the Commission, or employee of such contractor prepares, disseminates, or provides access to, any information pursuant to his employment or contract with the Commission, or his employment with such contractor.

[REDACTED]

~~SECRET~~ UNCLASSIFIED

SPECIFIED EXTERNAL DISTRIBUTION ONLY

January 1968

Exempt from CCRP Re-review Requirements
(per 7/22/82 Duff/Caudle memorandum)
N. Kinser 11-15-10

Classification cancelled (~~SECRET~~)

by authority of TID-1387 (Suppl.)

by EB DTIE, date 10/20/75
SC-PR-67-3023

SANDIA LABORATORIES QUARTERLY REPORT
AEROSPACE NUCLEAR SAFETY PROGRAM
OCTOBER 1 TO DECEMBER 31, 1967
(Title Unclassified)

Prepared by
Aerospace Nuclear Safety Department, 9310
V. E. Blake, Manager

Sandia Laboratory

Compiled by
R. G. Illing, 9319

NOTICE
This report was prepared as an account of work sponsored by the United States Government. Neither the United States nor the United States Energy Research and Development Administration, nor any of their employees, nor any of their contractors, subcontractors, or their employees, makes any warranty, express or implied, or assumes any legal liability or responsibility for the accuracy, completeness or usefulness of any information, apparatus, product or process disclosed, or represents that its use would not infringe privately owned rights.

LEGAL NOTICE
This report was prepared as an account of Government sponsored work. Neither the United States nor the Commission, nor any person acting on behalf of the Commission, makes any warranty or representation, expressed or implied, with respect to the accuracy, completeness, or usefulness of the information contained in this report, or the use of any information, apparatus, method, or process disclosed in this report, or that the use of any information, apparatus, method, or process disclosed in this report may not infringe privately owned rights, or that the use of any information, apparatus, method, or process disclosed in this report is for damages resulting from the use of any information, apparatus, method, or process disclosed in this report. As used in the above, "person acting on behalf of the Commission" includes any employee or contractor of the Commission, or employee of such contractor, to the extent that such employee or contractor of the Commission, or employee of such contractor prepares, disseminates, or provides access to, any information, apparatus, method, or process in connection with the Commission, or his employment with such contractor.

ABSTRACT

This report describes research, development, support, and test activities in the Sandia Laboratory Aerospace Nuclear Safety Program from October 1 to December 31, 1967.

~~GROUP 1 - Excluded from automatic downgrading and declassification.~~
~~This document contains restricted data as defined in the Atomic Energy Act of 1954, transmitted or to be transmitted in any manner in any form.~~

GROUP 1 - Excluded from automatic downgrading and declassification.

~~DISTRIBUTION OF THIS DOCUMENT IS LIMITED TO Government Agencies and Their Contractors~~

DISTRIBUTION OF THIS DOCUMENT IS UNLIMITED

BLANK

UNCLASSIFIED

SUMMARY

SNAP-19 Intact System

A meeting was held November 7 at Martin/Baltimore to discuss the flight dynamics of the intact reentry heat source (IRHS); it was agreed that the 0.30D chamfered ends on the IRHS might cause serious dynamic problems and that two modified configurations should be investigated. The reentry thermal analysis of the SNAP-19 generator and the IRHS was completed. Based on the results of these investigations, it was recommended on November 15 that the IRHS configuration be changed to the basic cylinder; this was accepted, and the design change was subsequently made.


The probability of the SNAP-19 impacting various areas, countries, and the largest cities of the world was estimated. Helium flow from a fueled capsule was observed; flow was a small percent of the theoretical helium generation rate at 1450°F. There appears to be a potential for helium storage within the fuel; further investigations are being coordinated.

SNAP-27

Heating rates to the GLFC ahead of the titanium struts were calculated for six flight conditions. The determination of the effect of surfaces and gaseous environments on the spontaneous ignition temperature of Aerozine 50 is continuing.

PLUTONIUM SYSTEMS SUPPORT

Four $^{238}\text{PuO}_2$ microspheres coated with 40 to 45 microns of pyrocarbon were tested in the Sandia 40-kW hyperthermal arc tunnel; the ablated debris is being analyzed by Tracerlab-West. The maximum percentages of melt which occur for fuel particles under various release conditions were calculated. Analytical studies are being conducted to calculate the quantity of helium retained within $^{238}\text{PuO}_2$ as well as to estimate the quantity released as a function of temperature.



Escape of Polonium from a Punctured Capsule

The results of the Mound polonium release experiment were analyzed; the analysis showed that the gross features are consistent with a simple diffusion model.

AMSA Capsule Impact Tests

A three-phase program was conducted to evaluate the impact resistance of the fuel capsule for the AMSA application.

OXIDATION OF ZIRCONIUM DROPLETS

Sandia and AeroChem Research Laboratories are jointly studying the combustion of single droplets of zirconium in oxygen-containing atmospheres; the program involves an analytical effort to develop a model that describes the temperature and reaction rate histories of the oxidizing droplets and which is consistent with earlier Sandia experimental work.

AUTOROTATION STUDIES

The general investigation of the dynamics and aerodynamics of autorotating bodies continued; various configurations were subsonically and hypersonically tested in wind tunnels in free-flight, one-degree-of-freedom, and supported modes.

AEC MEETING ON SEARCH, DETECTION, AND RECOVERY

The AEC Space Nuclear Systems Division will sponsor a meeting on the subject of search, detection, and recovery of radioisotope heat sources; Sandia Laboratory will host and assist in planning the meeting which will be held January 16 through 18, 1968.

[REDACTED]

UNCLASSIFIED

TABLE OF CONTENTS

SYSTEMS SUPPORT

Plutonium-Fueled Systems

	<u>Page</u>
SNAP-19	
SNAP-19 Dispersal System	9
SNAP-19 Intact System	9
Aerodynamic Analysis	9
Thermal Analysis	11
Heat Shield Burst Tests	15
Helium Retention	15
Land Impact Probabilities	16
Fuel Resuspension Analysis	17
Fuel Capsule Impact Tests	17
Interagency Review Panel Meeting and AEC Safety Evaluation Report	17

SNAP-27

Maximum Pressure Coefficient on GLFC During Reentry	32
Radiant Heat Test	32
Calculation of Heating Rates to GLFC Ahead of Titanium Struts	33
Spontaneous Ignition Temperature Studies	33
SNAP-27 Fire Model	35

PLUTONIUM SYSTEMS SUPPORT

Analytical Study of the Hypersonic Reentry of Small Spherical Particles	37
Stagnation Liquid Layer Ablation Study	37
Reentry Ablation Testing in a Hyperthermal Arc Tunnel	38
Analysis of Debris from Ablation of ²³⁸ PuO ₂ Microspheres in a Hyperthermal Arc Tunnel	41
Gas Gun Tests	43

[REDACTED]

[REDACTED]

TABLE OF CONTENTS
(continued)

	<u>Page</u>
40-kW Arc Jet Sampler	46
Formation of Plutonium Carbide	47
Release of Gases from PuO ₂	47
Melt Matrix Calculations	56
Fuel Simulant Studies	58
Fuel Fines from Impact	59
Solubility Studies	60
Correlation of Reported Plutonium Surface Air Concentrations with Measured Lung Burdens	62
Inhalation Studies	62

Polonium-Fueled Systems

SNAP-29

Polonium-210 in Soil	64
Force and Moment Tests	64
Escape of Polonium from a Punctured Capsule	65

Promethium-Fueled Systems

ADVANCED MANNED STRATEGIC AIRCRAFT (AMSA)

AMSA Capsule Impact Tests	66
-------------------------------------	----

[REDACTED]

TABLE OF CONTENTS
(continued)

ADVANCED TECHNOLOGY

Basic Studies

	<u>Page</u>
HIGH TEMPERATURE CHEMISTRY	67
OXIDATION OF ZIRCONIUM DROPLETS	67
INITIAL STAGES IN THE NITRIDATION OF METALS	70
ATMOSPHERIC DISPERSION STUDIES	71
Stardust Atmospheric Fallout Diagnostic Studies	71
AUTOROTATION STUDIES	71
FUEL PUCKS	72
CMA Computer Ablation Estimates	72
CAPSULE IMPACT	73
FUEL/CLAD/SOIL REACTION	74
SOIL CONDUCTIVITY	74
GENERAL STUDIES	74
Publication of SC-RR-67-232	74
DEMOGRAPHIC STUDIES	78
COMPUTER CODES	78
Computer Code HRS004	78
Martin FB-123 Computer Code	78
New Computer Codes	78
AEC MEETING ON SEARCH, DETECTION, AND RECOVERY OF RADIOISOTOPE HEAT SOURCES	79

Administrative

ESTABLISHMENT OF NEW STANDARD ANS DOCUMENT DISTRIBUTION	79
---	----

BLANK



SYSTEMS SUPPORT

Plutonium-Fueled Systems

SNAP-19

The SNAP-19 is a 30-watt thermoelectric generator. Two SNAP-19 generators will be mounted in tandem on the Nimbus B experimental weather satellite and will supplement the power generated by the satellite solar panels.

SNAP-19 Dispersal System (D. E. Randall)


The revised thermal model was completed. It incorporates radiation view factors for the finned generator and two-dimensional heat flow for a tumbling dispersal fuel capsule. The model is running with the HERMAN program, which provides temperature-time histories for specified thermal input functions. Results obtained to date for a few selected trajectories indicate that the fuel release points may occur at higher altitudes than was indicated by previous estimates. When the studies are completed, the results will be reported in detail.

SNAP-19 Intact System

The items reported under this heading concern the Intact Reentry Heat Source (IRHS) of the SNAP-19 system.

Aerodynamic Analysis (G. W. Stone)

Three configurations of cylinders representative of SNAP-19 capsules were tested at Mach 8 in free flight at the AEDC Wind Tunnel B on October 2, 1967. The configurations tested were the basic cylinder, the cylinder with 30-percent diameter end cuts at 90-degree relative roll position, and the IRHS cylinder with 30-percent diameter end cuts at 180-degree relative roll position. Each configuration was launched into the air stream in the end-on mode, side-on mode, and planar tumble mode



of motion. The model motions were recorded by high speed (5000 frames/sec) motion pictures.

The high speed motion pictures from this test were received from AEDC on October 30. The film showed that the model of the SNAP-19 IRHS exhibited a planar tumble motion in the plane of the chamfered corners at a rate of approximately 38 rps. Also, there appeared to be a slight acceleration during the short time of the test (0.2 sec). Neglecting the acceleration and assuming that the 38 rps was the steady-state autorotation rate of the model for the wind tunnel test conditions, the model tip speed ratio $\omega L/2V$, was calculated to be 0.007. This scaling parameter was assumed to be independent of Mach number at hypersonic speeds, and a steady-state autorotation rate of 90 rps was calculated for the full scale IRHS at a velocity of 20,000 fps during an orbital decay trajectory. This possible tumble rate is well above the structural capabilities of the capsule.

On November 7, a meeting was held at Martin/Baltimore to discuss the flight dynamics of the IRHS and to consider possible design changes from both dynamic and thermal viewpoints. Increasing dynamic pressure is extremely important during the reentry of symmetric missiles and reentry vehicles. Sandia presented an analytical technique that showed the energy input to the system caused by the chamfered ends on the IRHS and compared this energy input per cycle to the energy that is absorbed due to the increased dynamic pressure. This analysis showed further that, for the shallow reentry angles of an orbital decay or abort, the increasing atmospheric density was not capable of reducing the steady-state tumble rate, but that it was effective in increasing the time required for the capsule to reach steady-state.

This meeting also considered a possible problem at subsonic speeds, as indicated by test data taken on a SNAP-19 cylinder with 0.15 diameter end cuts during a July wind tunnel test at Edgewood Arsenal. We considered this test data to be qualitative at best because the model and its support blocked approximately 25 percent of the wind tunnel area.

As a result of this meeting, it was agreed that the 0.30 diameter chamfered ends on the SNAP-19 IRHS might cause several serious dynamic problems and that two modified configurations should be investigated.

If the capsule could withstand the side-on no-spin thermal environment of reentry, the SNAP-19 IRHS configuration should be changed to the basic cylinder; if, however, the thermal integrity of the capsule appeared to be marginal, the size of the end cuts should be reduced from 0.30 to 0.10 diameter. It was felt that the side-on no-spin condition for the basic cylinder was highly improbable. Also, it was felt that the 0.10 diameter end cuts would reduce the steady-state autorotation rate of the capsule to an acceptable level if the chamfered ends proved to be necessary.

On November 17-18, a hypersonic wind tunnel test of four cylindrical configurations was conducted at Mach 5, 7.3, and 11 in the SCARF VI 18-inch hypersonic wind tunnel at Sandia. The models tested were the basic SNAP-19 cylinder and the cylinder with 0.15, 0.30, and 0.45 diameter chamfered ends. The results of this test showed that the IRHS capsule with 0.30 diameter end cuts would tumble approximately 2.5 times as fast as indicated by the AEDC test (220 rps instead of 90 rps) at hypersonic speeds. This difference is due to the short test time at AEDC. The basic cylinder and the cylinder with 0.15 diameter end cuts did not autorotate during the test; however, the bearing friction in the support system was very high.

A subsonic wind tunnel test on the same four cylindrical configurations was conducted at Edgewood Arsenal on November 27. Test conditions were sea level density and air velocities from 0 to 200 mph. The results of this test showed that the SNAP-19 cylinder with 0.30 diameter end cuts could tumble at rates that exceed the structural capability of the capsule at subsonic speeds. Also, the test showed that the basic cylinder does not autorotate at subsonic speeds and that the cylinder with 0.15 diameter end cuts autorotates very slowly at subsonic speeds.

Based on results of these studies it was recommended that the IRHS configuration be changed to the basic cylinder. This recommendation was accepted, and the design change was subsequently made.

Thermal Analysis (R. D. Klett)

The reentry thermal analysis of the SNAP-19 generator and the IRHS was completed. Three-dimensional heat transfer and ablation programs

~~CONFIDENTIAL~~

were used to compute the thermal response of the system in space and during reentry with and without internal pressure and with oxidized and deoxidized interior metal surfaces. The configuration, motions, and trajectories analyzed were:

1. IRHS alone, randomly tumbling, orbital decay.
2. IRHS alone, side-on stable, orbital decay.
3. Generator on the Nimbus, end-over-end tumbling, orbital decay; IRHS with a random tumbling motion after release.
4. Generator on the Nimbus and Agena, end-over-end tumbling (the most severe reentry caused by guidance failure); IRHS with a random tumbling motion after release.

Results of the study show that the capsule will not melt in space regardless of internal pressure or surface conditions.

Figure 1 shows the parameter (\dot{m}/C_m) which governs the ablation rate as a function of surface temperature and pressure for the three ablation regimes. It can be seen that a catastrophic ablation failure would occur only if temperatures high enough to result in sublimation controlled ablation were achieved. Table I shows that the maximum temperature of the graphite remains at least 950°R below the sublimation controlled regime. Therefore, small errors in the heating rates would not change the predicted ablation depths significantly. Ablation depths for random tumbling reentry are insignificant. At the time of earth impact, the side-on stable IRHS will have ablated down to the center joint thread roots near the stagnation line. However, this depth of material removal is restricted to a 60-degree arc in the stagnation region. The maximum ablation depth on the aft side is 0.07 inch. The ablation rates are highest after the IRHS reaches high temperatures and the air density increases. It is important to note that only one-third of the total ablation will have taken place at the time of peak heating and only two-thirds at the completion of the aerodynamic heat pulse. A single rotation of the IRHS during reentry will reduce the circumferential ablation gradient greatly, and the maximum ablation depth will not be much greater than that predicted for a random tumbling-spinning reentry.

~~CONFIDENTIAL~~

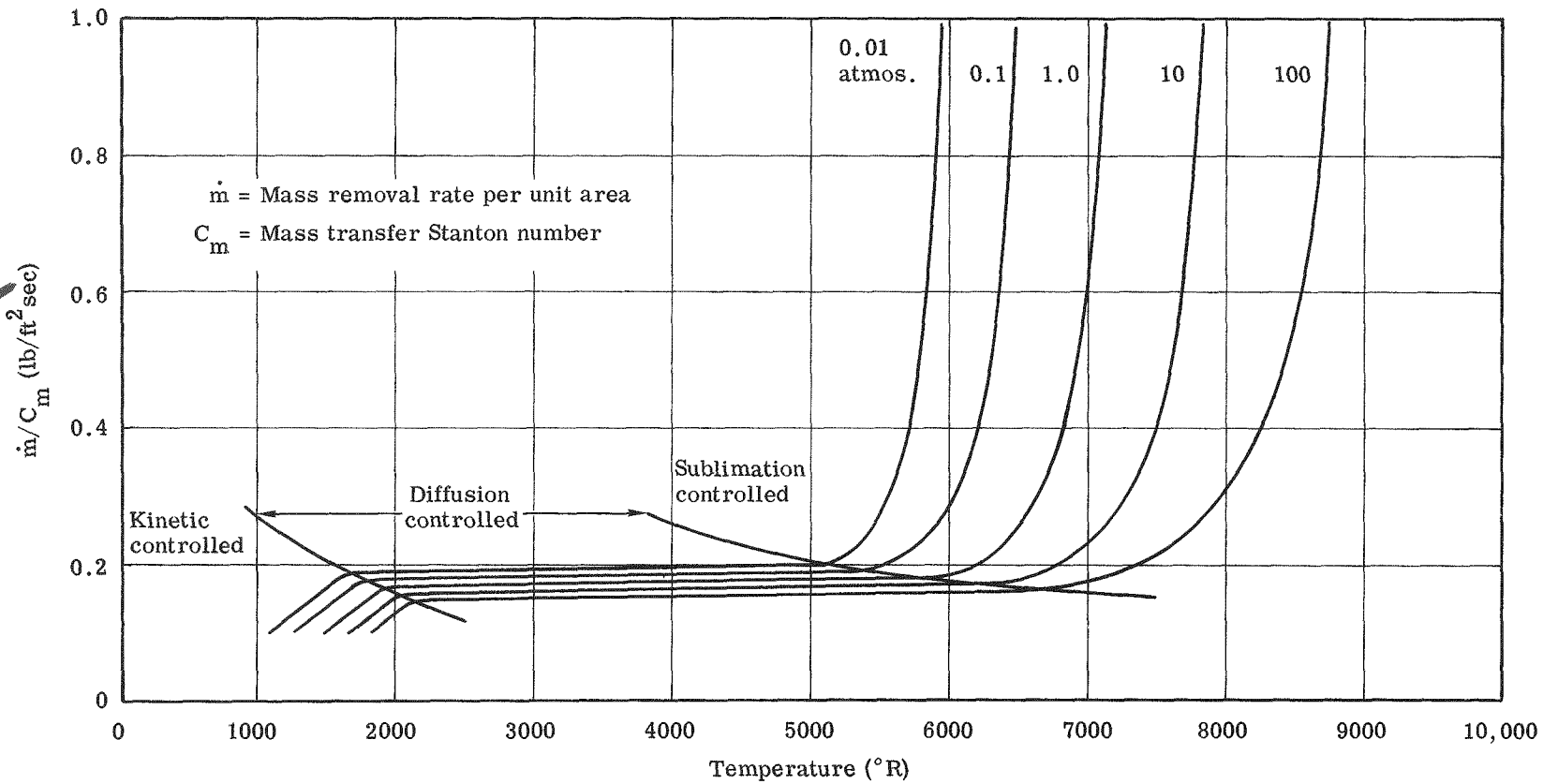


Figure 1. Ablation rate parameter of graphite as a function of temperature and pressure (D67-15955)



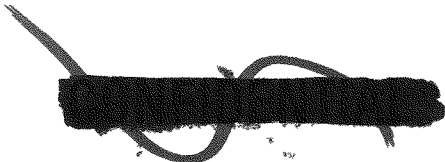
TABLE I


Maximum Ablation and Temperatures of the IRHS
During Orbital Decay (D67-15956)

<u>Parameter</u>	<u>Side-On Stable</u>	<u>Random Tumble Spin</u>
<u>Ablation Material</u>		
Maximum temperature	4610°R	3668°R
Impact temperature	1988°R	2062°R
ΔT below sublimation temperature at T maximum	950°R	1580°R
Ablation at \dot{q} maximum	0.0676 in.	0.0251 in.
Ablation at end of heat pulse	0.128 in.	0.0450 in.
Ablation at earth impact	0.171 in.	0.0625 in.
<u>Liner</u>		
Maximum temperature	4394°R	3510°R
Impact temperature	2007°R	2122°R
ΔT below melting temperature at T maximum	1491°R	2375°R
<u>Capsule</u>		
Maximum temperature	4394°R	3524°R
Impact temperature	2748°R	2835°R
ΔT above melting temperature at T maximum	1510°R	640°R
<u>Fuel</u>		
Maximum temperature	4394°R	3524°R
Impact temperature	2748°R	2835°R
ΔT below melting temperature at T maximum	129°R	999°R

For either mode of reentry, the liner and fuel will not melt, and the capsule will melt and resolidify before earth impact. For the stable orientation, the fuel at the outer surface (in contact with the liner) at the stagnation line will reach a temperature 129°R below the fuel melt temperature for a few seconds.

Preliminary data from the side-on stable plasma jet tests of the IRHS conducted at Martin the week of November 6 indicated that the IRHS will survive reentry in this most severe orientation. However, the tests





do not simulate flight conditions closely enough to qualify as proof tests. The prime function of the tests will be to substantiate the analytical studies.

Fuel temperatures of the IRHS fuel during reentry from orbit and during a guidance failure abort were furnished to all organizations engaged in helium release studies.

Martin-Marietta was supplied with aeroheating data reduced from the basic data obtained from shock tunnel cylinder tests performed by Cornell Aeronautical Laboratory under Sandia contract. The heating profile for the entire surface of an $L/D = 2$ cylinder in cross flow and the average local heating ratios for a spinning cylinder as a function of angle of attack were included.

Heat Shield Burst Tests (J. D. Boyd)

Three SNAP-19 IRHS heat shield assemblies were subjected to an internal hydrostatic pressure test to determine the failure pressure and mode. Two of the test assemblies were fabricated by Sandia of ATJ graphite. These two units failed at the thread relief of the male thread, at 380 and 346 psi. Predicted failure pressure, ignoring any notch factor, was 382 psi.

The third test assembly was fabricated by Martin-Marietta Corporation of POCO graphite and was of flight quality, except that no internal coating had been applied. The POCO unit failed at the thread relief of the female thread. Hydrostatic failure pressure was 480 psi. Prior to the failure test, the POCO assembly underwent a helium leak check. The leak rate of the entire graphite heat shield was 3.6 cc/sec with a pressure differential of one atmosphere.

Helium Retention (R. E. Berry)

A plugging effect was observed during Mound Laboratory's evaluation of the ability of the Haynes-25 frit filter to pass helium gas generated in the fuel. To obtain information on whether the plugging was produced by the test methods or would occur during actual conditions,

[REDACTED]

a fueled capsule was placed under test. The helium flow from this capsule was observed to be a small percent of the theoretical helium generation rate when held at a constant temperature of 1450°F. Also, when the capsule was stored overnight at a reduced temperature and returned to test at 1450°F the following morning, a pressure spike or increased helium flow was noted with a return to the small percent of theoretical generation rate after several minutes. This phenomenon initiated the investigation of helium storage within the fuel. A literature search and preliminary calculations performed at Sandia revealed a potential for helium storage of about 96 percent at ambient temperature. Because the fueled capsule helium release rate could be attributed to either a plugged filter or helium storage, additional tests were initiated at Mound to investigate the problem.

One gram of fuel has been under test for an extended period of time, and again a small percent of the theoretical helium generated is being released from the sample. This indicates helium storage within the fuel.

Helium storage creates a second problem because a sudden or instantaneous release of the stored helium could cause a high internal pressure and might rupture the graphite heat shield during reentry. The release of the stored helium probably occurs as a function of time and temperature. The necessary activation energies and diffusion coefficients for PuO_2 are not available to predict the helium release rate. Experiments are being planned at both Mound Research Laboratory and at Los Alamos Scientific Laboratory to establish these fuel characteristics. (See also the item "Release of Gases from PuO_2 " on page 55.)

Land Impact Probabilities (L. A. Hanchey)

The probabilities of the SNAP-19 impacting various areas, countries, and the largest cities of the world were estimated. The probabilities were calculated for the system as it sits on the launch pad and as it reenters from polar orbit. The second case is generalized and is applicable to any object reentering from a polar orbit. The probabilities included corrections for proportionate areas in the various latitude belts and for the probability of impacting the various

~~CONFIDENTIAL~~

latitude belts, as previously computed in SC-RR-66-41.* The results of this study are given in Tables II through XI.

Fuel Resuspension Analysis (L. A. Hanchey)

A letter was sent to the AEC Safety Branch on October 6 outlining the results of a study on the resuspension hazard from the intact SNAP-19. The study includes estimates of probabilities of impacting various surfaces in areas of different population density, and an analysis of the applicability of the Air Force permissible ground contamination levels.

Fuel Capsule Impact Tests (F. L. Baker)

Four SNAP-19 IRHS capsules were drop-tested at the Tonopah Test Range (TTR) to obtain a preliminary indication of the fuel dispersion resulting from post reentry impact. A report containing photographs of the impacted capsules and pertinent test data was published.**

Interagency Review Panel Meeting and AEC Safety Evaluation Report (L. A. Hanchey)

Sandia representatives provided technical support to the AEC during a meeting of the Interagency Review Panel in Washington, D. C., on October 30; the meeting was held to review the safety of the SNAP-19 intact system. The AEC Safety Evaluation Report on the intact SNAP-19, dated October 24, was reviewed by Sandia and comments were provided to AEC Headquarters.

* SC-RR-66-41, Probability Distributions of Latitudes of Reentry and Impact Following Decay of Polar Orbits, T. S. Edrington, Sandia Laboratory, Albuquerque, New Mexico, March 1966.

** SC-DR-67-826, SNAP-19 Exploratory Postreentry Impact Dispersion Test, F. L. Baker, Sandia Laboratory, Albuquerque, New Mexico, September 1967, CRD.

~~CONFIDENTIAL~~

TABLE II
Probabilities of Impacting Areas of the World

Zone	Area ¹ (sq mi)	Effective Area ¹ (sq mi)	Impact Probability ² (Given Reentry from Polar Orbit)	Impact Probability ³ (SNAP-19, Prelaunch)
Africa	11,710,517	7,606,506	3.9×10^{-2}	6.2×10^{-4}
Asia	6,014,342	4,190,757	2.1×10^{-2}	3.4×10^{-4}
South America	6,863,982	4,513,522	2.3×10^{-2}	3.7×10^{-4}
Middle America	1,046,611	704,677	3.6×10^{-3}	5.7×10^{-5}
Europe	1,483,186	1,705,276	8.7×10^{-3}	1.4×10^{-4}
Sino-Soviet	13,434,642	14,845,621	7.5×10^{-2}	1.2×10^{-3}
Anglo North America	7,467,020	8,433,014	4.3×10^{-2}	6.8×10^{-4}
Ocean Countries	3,395,857	2,612,722	1.3×10^{-2}	2.1×10^{-4}
Total	51,416,157	44,612,095	2.3×10^{-1}	3.6×10^{-3}

¹Taken from Tables III through X.

²Impact probability = $\frac{\text{effective area}}{\text{earth's surface area}}$.

³Impact probability = $\left(\frac{\text{effective area}}{\text{earth's surface area} = 1.97 \times 10^8 \text{ square miles}} \right) \times \left(\begin{array}{l} \text{Probability of SNAP-19} \\ \text{getting in a short} \\ \text{orbit} = 0.016 \end{array} \right)$.

TABLE III

(D68-11014)

Probabilities of Impacting Countries in Africa

Country	Area ¹ (sq mi)	Approximate Latitude Range	Area Correction ² Divisor	Effective Area (sq mi)	Impact Probability ³ (Given Reentry from Polar Orbit)	Impact Probability ⁴ (SNAP-19, Prelaunch)
Algeria	919,591	19 - 37°N	1.32	696,660	3.5×10^{-3}	5.7×10^{-5}
British Africa	275,000	17 - 27°S	1.44	190,972	9.7×10^{-4}	1.6×10^{-5}
	11,716	30°S	1.29	9,082	4.6×10^{-5}	7.4×10^{-7}
	6,704	26°S	1.35	4,966	2.5×10^{-5}	4.0×10^{-7}
Burundi	10,747	3°S	1.74	6,176	3.1×10^{-5}	5.0×10^{-7}
Cameroon	183,568	2 - 10°N	1.72	106,726	5.4×10^{-4}	8.7×10^{-6}
Central African Rep.	236,293	4 - 10°N	1.71	138,183	7.0×10^{-4}	1.1×10^{-5}
Chad	495,753	8 - 24°N	1.59	311,794	1.6×10^{-3}	2.5×10^{-5}
Congo (Brazzaville)	132,046	4°S - 4°N	1.75	75,455	3.8×10^{-4}	6.1×10^{-6}
Congo (Leopoldville)	905,563	5°N - 12°S	1.74	520,439	2.6×10^{-3}	4.2×10^{-5}
Dahomey	43,483	7 - 12°N	1.67	26,038	1.3×10^{-4}	2.1×10^{-6}
Ethiopia	457,266	4 - 18°N	1.66	275,461	1.4×10^{-3}	2.2×10^{-5}
French Africa	8,494	12°N	1.66	5,117	2.6×10^{-5}	4.2×10^{-7}
Gabon	102,089	3°S - 2°N	1.75	58,337	3.0×10^{-4}	4.7×10^{-6}
Gambia	4,004	13°N	1.64	2,441	1.2×10^{-5}	2.0×10^{-7}
Ghana	92,099	5 - 11°N	1.70	54,176	2.8×10^{-4}	4.4×10^{-6}
Guinea	94,925	8 - 12°N	1.67	56,841	2.9×10^{-4}	4.6×10^{-6}
Ivory Coast	124,503	5 - 10°N	1.70	73,237	3.7×10^{-4}	5.9×10^{-6}
Kenya	224,960	4°S - 5°N	1.75	128,549	6.5×10^{-4}	1.0×10^{-5}

TABLE III (cont)

(D68-11015)

<u>Country</u>	<u>Area¹ (sq mi)</u>	<u>Approximate Latitude Range</u>	<u>Area Correction² Divisor</u>	<u>Effective Area (sq mi)</u>	<u>Impact Probability³ (Given Reentry from Polar Orbit)</u>	<u>Impact Probability⁴ (SNAP-19, Prelaunch)</u>
Liberia	43,000	5 - 8°N	1.71	25,146	1.3×10^{-4}	2.0×10^{-6}
Libya	679,359	20 - 32°N	1.35	503,229	2.6×10^{-3}	4.1×10^{-5}
Malagasy Rep.	230,035	12 - 25°N	1.53	150,350	7.6×10^{-4}	1.2×10^{-5}
Malawi	46,066	10 - 17°S	1.63	28,261	1.4×10^{-4}	2.3×10^{-6}
Mali	463,948	10 - 25°N	1.55	299,321	1.5×10^{-3}	2.4×10^{-5}
Mauritania	419,231	15 - 27°N	1.47	285,191	1.4×10^{-3}	2.3×10^{-5}
Morocco	171,834	28 - 35°N	1.27	135,302	6.7×10^{-4}	1.1×10^{-5}
Niger	489,189	14 - 23°N	1.53	319,731	1.6×10^{-3}	2.6×10^{-5}
Nigeria	356,669	4 - 14°N	1.68	212,303	1.1×10^{-3}	1.7×10^{-5}
Portuguese Africa						
Guinea	13,948	8°N	1.69	8,253	4.2×10^{-5}	6.7×10^{-7}
Angola	481,351	5 - 18°S	1.66	289,970	1.5×10^{-3}	2.4×10^{-5}
Mozambique	302,328	10 - 25°S	1.55	195,050	9.9×10^{-4}	1.6×10^{-5}
Rhodesia	150,333	15 - 22°S	1.54	97,619	5.0×10^{-4}	7.9×10^{-6}
Rwanda	10,169	2°S	1.74	5,844	3.0×10^{-5}	4.7×10^{-7}
Senegal	75,750	12 - 16°N	1.62	46,759	2.4×10^{-4}	3.8×10^{-6}
Sierra Leone	27,699	8 - 10°N	1.68	16,488	8.4×10^{-5}	1.3×10^{-6}
Somali Rep.	246,201	1°S - 12°N	1.73	142,313	7.2×10^{-4}	1.2×10^{-5}
Spanish Africa	102,703	22 - 28°N	1.37	74,966	3.8×10^{-4}	6.1×10^{-6}
Rio Muni	10,831	2°N	1.74	6,225	3.2×10^{-5}	5.1×10^{-7}

TABLE III (cont)

(D68-11016)

Country	Area ¹ (sq mi)	Approximate Latitude Range	Area Correction ² Divisor	Effective Area (sq mi)	Impact Probability ³ (Given Reentry from Polar Orbit)	Impact Probability ⁴ (SNAP-19, Prelaunch)
South Africa	471,445	22 - 35°S	1.31	359,882	1.8×10^{-3}	2.9×10^{-5}
Southwest Africa	317,887	17 - 29°S	1.42	223,864	1.1×10^{-3}	1.8×10^{-5}
Sudan	967,500	4 - 22°N	1.63	593,558	3.0×10^{-3}	4.8×10^{-5}
Tanzania	362,819	2 - 12°S	1.71	212,175	1.1×10^{-3}	1.7×10^{-5}
Togo	21,853	6 - 11°N	1.69	12,931	6.6×10^{-5}	1.1×10^{-6}
Tunisia	48,332	30 - 37°N	1.23	39,294	2.0×10^{-4}	3.2×10^{-6}
Uganda	91,134	0 - 4°N	1.74	52,376	2.7×10^{-4}	4.3×10^{-6}
UAR	386,100	22 - 32°N	1.34	288,134	1.5×10^{-3}	2.3×10^{-5}
Upper Volta	105,869	10 - 15°N	1.64	64,554	3.3×10^{-4}	5.2×10^{-6}
Zambia	288,130	8 - 18°S	1.63	176,767	9.0×10^{-4}	1.4×10^{-5}
Total	11,710,517			7,606,506	3.9×10^{-2}	6.2×10^{-4}

¹Per 1966 National Geographic Atlas.

²Function of proportionate area in latitude range and impact probability in latitude range (SC-RR-66-41).

³Impact probability = $\frac{\text{effective area}}{\text{earth's surface area}}$.

⁴Impact probability = $\left(\frac{\text{effective area}}{\text{earth's surface area} = 1.97 \times 10^8 \text{ square miles}} \right) \times \left(\begin{array}{l} \text{Probability of SNAP-19} \\ \text{getting in a short} \\ \text{orbit} = 0.016 \end{array} \right)$.

TABLE IV

(D68-11017)

Probabilities of Impacting Countries in Asia

Country	Area ¹ (sq mi)	Approximate Latitude Range	Area Correction ² Divisor	Effective Area (sq mi)	Impact Probability ³ (Given Reentry from Short Orbit)	Impact Probability ⁴ (SNAP-19, Prelaunch)
Afghanistan	253,861	30 - 40°N	1.21	209,802	1.1×10^{-3}	1.7×10^{-5}
Bhutan	18,147	20 - 30°N	1.37	13,246	6.7×10^{-5}	1.1×10^{-6}
Burma	261,789	10 - 30°N	1.49	175,697	8.9×10^{-4}	1.4×10^{-5}
Cambodia	69,898	10 - 15°N	1.64	42,621	2.2×10^{-4}	3.5×10^{-6}
Ceylon	25,332	5 - 10°N	1.70	14,901	7.6×10^{-5}	1.2×10^{-6}
China, Rep. (Taiwan)	13,885	22 - 26°N	1.39	9,989	5.1×10^{-5}	8.1×10^{-7}
Cyprus	3,572	35°N	1.21	2,952	1.5×10^{-5}	2.4×10^{-7}
India	1,176,151	10 - 30°N	1.49	789,363	4.0×10^{-3}	6.4×10^{-5}
Indonesia	575,893	10°S - 5°N	1.75	329,082	1.7×10^{-3}	2.7×10^{-5}
Iran	636,293	25 - 40°N	1.25	509,034	2.6×10^{-3}	4.1×10^{-5}
Iraq	173,259	30 - 37°N	1.23	140,861	7.2×10^{-4}	1.1×10^{-5}
Israel	7,993	35°N	1.21	6,606	3.4×10^{-5}	5.4×10^{-7}
Japan	142,726	30 - 45°N	1.17	121,988	6.2×10^{-4}	9.9×10^{-6}
Jordan	34,820	30 - 34°N	1.26	27,635	1.4×10^{-4}	2.2×10^{-6}
South Korea	38,004	34 - 38°N	1.19	31,936	1.6×10^{-4}	2.6×10^{-6}
Kuwait	6,178	29 - 30°N	1.30	4,752	2.4×10^{-5}	3.9×10^{-7}
Laos	91,429	15 - 22°N	1.53	59,756	3.0×10^{-4}	4.9×10^{-6}
Lebanon	4,015	35°N	1.21	3,318	1.7×10^{-5}	2.7×10^{-7}
Malaysia	128,430	1 - 7°N	1.74	73,810	3.7×10^{-4}	6.0×10^{-6}

TABLE IV (cont)

(D68-11018)

Country	Area ¹ (sq mi)	Approximate Latitude Range	Area Correction ² Divisor	Effective Area (sq mi)	Impact Probability ³ (Given Reentry from Short Orbit)	Impact Probability ⁴ (SNAP-19, Prelaunch)
Nepal	54,362	27 - 30°N	1.31	41,498	2.1×10^{-4}	3.4×10^{-6}
Pakistan	365,528	22 - 37°N	1.30	281,175	1.4×10^{-3}	2.3×10^{-5}
Philippines	115,830	5 - 19°N	1.65	70,200	3.6×10^{-4}	5.7×10^{-6}
Thailand	198,456	12 - 20°N	1.59	124,815	6.3×10^{-4}	1.0×10^{-5}
Turkey	301,381	36 - 42°N	1.14	264,369	1.3×10^{-3}	2.1×10^{-5}
South Vietnam	65,948	8 - 17°N	1.64	40,212	2.0×10^{-4}	3.3×10^{-6}
Saudi Arabia	870,000	12 - 32°N	1.44	604,167	3.1×10^{-3}	4.9×10^{-5}
States of Arabian Peninsula	234,375	12 - 26°N	1.52	154,194	7.8×10^{-4}	1.3×10^{-5}
Syria	71,498	35°N	1.21	59,089	3.0×10^{-4}	4.8×10^{-6}
Yemen	75,289	13 - 17°N	1.61	46,763	2.4×10^{-4}	3.8×10^{-6}
Total	6,014,342			4,190,757	2.1×10^{-2}	3.4×10^{-4}

¹Per 1966 National Geographic Atlas.

²Function of proportionate area in latitude range and impact probability in latitude range (SC-RR-66-41).

³Impact probability = $\frac{\text{effective area}}{\text{earth's surface area}}$.

⁴Impact probability = $\left(\frac{\text{effective area}}{\text{earth's surface area} = 1.97 \times 10^8 \text{ square miles}} \right) \times \left(\begin{array}{l} \text{Probability of SNAP-19} \\ \text{getting in a short} \\ \text{orbit} = 0.016 \end{array} \right)$.

TABLE V

(D68-11019)

Probabilities of Impacting Countries in South America

Country	Area ¹ (sq mi)	Approximate Latitude Range	Area Correction ² Divisor	Effective Area (sq mi)	Impact Probability ³ (Given Reentry from Polar Orbit)	Impact Probability ⁴ (SNAP-19, Prelaunch)
Argentina	1,072,068	20 - 55°S	1.18	908,532	4.6×10^{-3}	7.4×10^{-5}
Bolivia	424,163	10 - 25°S	1.52	279,055	1.4×10^{-3}	2.3×10^{-5}
Brazil	3,286,473	5°N - 30°S	1.64	2,003,947	1.0×10^{-2}	1.6×10^{-4}
Chile	286,396	20 - 55°S	1.18	242,708	1.2×10^{-3}	2.0×10^{-5}
Colombia	439,513	5°S - 10°N	1.75	251,150	1.3×10^{-3}	2.0×10^{-5}
Ecuador	104,506	0 - 5°S	1.75	59,718	3.0×10^{-4}	4.9×10^{-6}
Paraguay	157,047	20 - 25°S	1.43	109,823	5.6×10^{-4}	8.9×10^{-6}
Peru	496,222	0 - 20°S	1.67	297,139	1.5×10^{-3}	2.4×10^{-5}
Uruguay	72,172	30 - 35°S	1.25	57,738	2.9×10^{-4}	4.7×10^{-6}
Venezuela	352,143	0 - 10°N	1.73	203,551	1.0×10^{-3}	1.7×10^{-5}
Guianas	55,144	0 - 10°N	1.73	31,875	1.6×10^{-4}	2.6×10^{-6}
	83,000		1.73	47,977	2.4×10^{-4}	3.9×10^{-6}
	35,135		1.73	20,309	1.0×10^{-4}	1.6×10^{-6}
Total	6,863,982			4,513,522	2.3×10^{-2}	3.7×10^{-4}

¹Per 1966 National Geographic Atlas.

²Function of proportionate area in latitude range and impact probability in latitude range (SC-RR-66-41).

³Impact probability = $\frac{\text{effective area}}{\text{earth's surface area}}$.

⁴Impact probability = $\left(\frac{\text{effective area}}{\text{earth's surface area} = 1.97 \times 10^8 \text{ square miles}} \right) \times \left(\text{Probability of SNAP-19 getting in a short orbit} = 0.016 \right)$.

TABLE VI

(D68-11020)

Probabilities of Impacting Countries in Middle America

Country	Area ¹ (sq mi)	Approximate Latitude Range	Area Correction ² Divisor	Effective Area (sq mi)	Impact Probability ³ (Given Reentry from Short Orbit)	Impact Probability ⁴ (SNAP-19, Prelaunch)
British Honduras	8,867	17°N	1.56	5,684	2.9×10^{-5}	4.6×10^{-7}
Costa Rica	19,575	10°N	1.67	11,722	6.0×10^{-5}	9.5×10^{-7}
Cuba	44,218	20 - 25°N	1.43	30,922	1.6×10^{-4}	2.5×10^{-6}
Dominican Republic	18,816	15 - 20°N	1.55	12,139	6.2×10^{-5}	9.9×10^{-7}
El Salvador	8,260	15°N	1.61	5,130	2.6×10^{-5}	4.2×10^{-7}
Guatemala	42,042	15°N	1.61	26,113	1.3×10^{-4}	2.1×10^{-6}
Honduras	43,277	15°N	1.61	26,880	1.4×10^{-4}	2.2×10^{-6}
Jamaica	4,232	18°N	1.54	2,748	1.4×10^{-5}	2.2×10^{-7}
Mexico	761,600	15 - 30°N	1.45	525,241	2.7×10^{-3}	4.3×10^{-5}
Nicaragua	53,938	10 - 15°N	1.64	32,889	1.7×10^{-4}	2.7×10^{-6}
Panama	29,208	5 - 10°N	1.70	17,181	8.7×10^{-5}	1.4×10^{-6}
Trinidad and Tobago	1,864	10°N	1.67	1,116	5.7×10^{-6}	9.1×10^{-8}
Haiti	10,714	15 - 20°N	1.55	6,912	3.5×10^{-5}	5.6×10^{-7}
Total	1,046,611			704,677	3.6×10^{-3}	5.7×10^{-5}

¹Per 1966 National Geographic Atlas.

²Function of proportionate area in latitude range and impact probability in latitude range (SC-RR-66-41).

³Impact probability = $\frac{\text{effective area}}{\text{earth's surface area}}$.

⁴Impact probability = $\left(\frac{\text{effective area}}{\text{earth's surface area} = 1.97 \times 10^8 \text{ square miles}} \right) \times \left(\text{Probability of SNAP-19 getting in a short orbit} = 0.016 \right)$.

TABLE VII

(D68-11021)

Probabilities of Impacting Countries in Europe

Country	Area ¹ (sq mi)	Approximate Latitude Range	Area Correction ² Divisor	Effective Area (sq mi)	Impact Probability ³ (Given Reentry from Polar Orbit)	Impact Probability ⁴ (SNAP-19, Prelaunch)
Austria	32,374	47 - 49°N	0.99	32,701	1.7×10^{-4}	2.7×10^{-6}
Belgium	11,781	50 - 52°N	0.93	12,668	6.4×10^{-5}	1.0×10^{-6}
Denmark	16,619	55 - 58°N	0.83	20,023	1.0×10^{-4}	1.6×10^{-6}
Finland	130,119	60 - 70°N	0.64	203,311	1.0×10^{-3}	1.7×10^{-5}
France	211,207	42 - 51°N	1.01	209,116	1.1×10^{-3}	1.7×10^{-5}
West Germany	95,742	48 - 55°N	0.92	104,067	5.3×10^{-4}	8.5×10^{-6}
Greece	50,994	35 - 42°N	1.15	44,343	2.3×10^{-4}	3.6×10^{-6}
Iceland	39,768	64 - 66°N	0.64	62,138	3.2×10^{-4}	5.0×10^{-6}
Ireland	27,135	52 - 55°N	0.89	30,489	1.5×10^{-4}	2.5×10^{-6}
Italy	116,303	37 - 47°N	1.09	106,700	5.4×10^{-4}	8.7×10^{-6}
Netherlands	12,978	52 - 54°N	0.90	14,420	7.3×10^{-5}	1.2×10^{-6}
Norway	125,181	58 - 70°N	0.66	189,668	9.6×10^{-4}	1.5×10^{-5}
Portugal	35,510	37 - 42°N	1.13	31,425	1.6×10^{-4}	2.6×10^{-6}
Spain	194,883	35 - 45°N	1.12	174,003	8.8×10^{-4}	1.4×10^{-5}
Sweden	173,665	55 - 70°N	0.69	251,688	1.3×10^{-3}	2.0×10^{-5}

TABLE VII (cont)

(D68-11022)

Country	Area ¹ (sq mi)	Approximate Latitude Range	Area Correction ² Divisor	Effective Area (sq mi)	Impact Probability ³ (Given Reentry from Polar Orbit)	Impact Probability ⁴ (SNAP-19, Prelaunch)
Switzerland	15,941	46 - 47° N	1.01	15,783	8.0×10^{-5}	1.3×10^{-6}
UK	94,220	50 - 60° N	0.86	109,558	5.6×10^{-4}	8.9×10^{-6}
Yugoslavia	98,766	41 - 47° N	1.06	93,175	4.7×10^{-4}	7.6×10^{-6}
Total	1,483,186			1,705,276	8.7×10^{-3}	1.4×10^{-4}

¹Per 1966 National Geographic Atlas.

²Function of proportionate area in latitude range and impact probability in latitude range (SC-RR-66-41).

³Impact probability = $\frac{\text{effective area}}{\text{earth's surface area}}$.

⁴Impact probability = $\left(\frac{\text{effective area}}{\text{earth's surface area} = 1.97 \times 10^8 \text{ square miles}} \right) \times \left(\begin{array}{l} \text{Probability of SNAP-19} \\ \text{getting in a short} \\ \text{orbit} = 0.016 \end{array} \right)$.

TABLE VIII

(D68-11023)

Probabilities of Impacting Sino-Soviet Bloc Countries

Country	Area ¹ (sq mi)	Approximate Latitude Range	Area Correction ² Divisor	Effective Area (sq mi)	Impact Probability ³ (Given Reentry from Polar Orbit)	Impact Probability ⁴ (SNAP-19, Prelaunch)
Albania	11,100	40 - 42°N	1.11	10,000	5.1×10^{-5}	8.1×10^{-7}
Bulgaria	42,729	41 - 44°N	1.08	39,564	2.0×10^{-4}	3.2×10^{-6}
Czechoslovakia	49,370	48 - 52°N	0.95	51,968	2.6×10^{-4}	4.2×10^{-6}
East Germany	41,659	50 - 54°N	0.91	45,779	2.3×10^{-4}	3.7×10^{-6}
Hungary	35,919	46 - 48°N	1.00	35,919	1.8×10^{-4}	2.9×10^{-6}
Poland	120,664	49 - 55°N	0.91	132,598	6.7×10^{-4}	1.1×10^{-5}
Rumania	91,700	43 - 48°N	1.03	89,029	4.5×10^{-4}	7.2×10^{-6}
China, People's Rep.	3,691,506	20 - 55°N	1.17	3,155,133	1.6×10^{-2}	2.6×10^{-4}
North Korea	46,540	38 - 42°N	1.12	41,554	2.1×10^{-4}	3.4×10^{-6}
Mongolia	592,664	42 - 52°N	1.00	592,664	3.0×10^{-3}	4.8×10^{-5}
USSR	8,649,498	35 - 80°N	0.815	10,610,277	5.4×10^{-2}	8.6×10^{-4}
North Vietnam	61,293	17 - 23°N	1.49	41,136	2.1×10^{-4}	3.3×10^{-6}
Total	13,434,642			14,845,621	7.5×10^{-2}	1.2×10^{-3}

¹Per 1966 National Geographic Atlas.

²Function of proportionate area in latitude range and impact probability in latitude range (SC-RR-66-41).

³Impact probability = $\frac{\text{effective area}}{\text{earth's surface area}}$.

⁴Impact probability = $\left(\frac{\text{effective area}}{\text{earth's surface area} = 1.97 \times 10^8 \text{ square miles}} \right) \times \left(\begin{array}{l} \text{Probability of SNAP-19} \\ \text{getting in a short} \\ \text{orbit} = 0.016 \end{array} \right)$.

TABLE IX

(D68-11024)

Probabilities of Impacting Anglo North American Countries

<u>Country</u>	<u>Area¹ (sq mi)</u>	<u>Approximate Latitude Range</u>	<u>Area Correction² Divisor</u>	<u>Effective Area (sq mi)</u>	<u>Impact Probability³ (Given Reentry from Polar Orbit)</u>	<u>Impact Probability⁴ (SNAP-19, Prelaunch)</u>
Canada	3,851,809	50 - 70°N	0.74	5,205,147	2.6×10^{-2}	4.3×10^{-4}
United States	3,615,211	30 - 50°N	1.12	3,227,867	1.6×10^{-2}	2.6×10^{-4}
Total	7,467,020			8,433,014	4.3×10^{-2}	6.8×10^{-4}

¹Per 1966 National Geographic Atlas.

²Function of proportionate area in latitude range and impact probability in latitude range (SC-RR-66-41).

³Impact probability = $\frac{\text{effective area}}{\text{earth's surface area}}$.

⁴Impact probability = $\left(\frac{\text{effective area}}{\text{earth's surface area} = 1.97 \times 10^8 \text{ square miles}} \right) \times \left(\begin{array}{l} \text{Probability of SNAP-19} \\ \text{getting in a short} \\ \text{orbit} = 0.016 \end{array} \right)$.

TABLE X

(D68-11025)

Probabilities of Impacting in Ocean Countries

Country	Area ¹ (sq mi)	Approximate Latitude Range	Area Correction ² Divisor	Effective Area (sq mi)	Impact Probability ³ (Given Reentry from Polar Orbit)	Impact Probability ⁴ (SNAP-19, Prelaunch)
Australia	2,974,581	12 - 40°S	1.35	2,203,393	1.1×10^{-2}	1.8×10^{-4}
New Guinea	183,540	3 - 10°S	1.71	107,333	5.4×10^{-4}	8.7×10^{-6}
Greenland ⁵	134,000	60 - 70°N	0.64	209,375	1.1×10^{-3}	1.7×10^{-5}
New Zealand	103,736	35 - 45°S	1.12	92,621	4.7×10^{-4}	7.5×10^{-6}
Total	3,395,857			2,612,722	1.3×10^{-2}	2.1×10^{-4}

¹Per 1966 National Geographic Atlas.

²Function of proportionate area in latitude range and impact probability in latitude range (SC-RR-66-41).

³Impact probability = $\frac{\text{effective area}}{\text{earth's surface area}}$.

⁴Impact probability = $\left(\frac{\text{effective area}}{\text{earth's surface area} = 1.97 \times 10^8 \text{ square miles}} \right) \times \left(\begin{array}{l} \text{Probability of SNAP-19} \\ \text{getting in a short} \\ \text{orbit} = 0.016 \end{array} \right)$.

⁵Sixteen percent of Greenland stated not to be ice--assumed to be 60 to 70-degree belt. Actual area = 840,000 sq mi.

TABLE XI

(D68-11026)

Probabilities of An Object Impacting Large Cities

City ¹	Population ² (people x 10 ³)	Area ² (sq mi)	Population Density (people/ sq mi)	Latitude	Area Correction ³ Divisor	Effective Area (sq mi)	Impact Probability ⁴ (Given Reentry from Polar Orbit)	Impact Probability ⁵ (SNAP-19, Prelaunch)
Tokyo/Yokohama	17,403	398	43,726	35°N	1.21	329	1.7×10^{-6}	2.7×10^{-8}
New York	15,663	1705	9,186	40°N	1.12	1522	7.7×10^{-6}	1.2×10^{-7}
London	8,699	620	14,030	51°N	0.93	667	3.4×10^{-6}	5.4×10^{-8}
Los Angeles	8,161	1317	6,196	34°N	1.23	1071	5.4×10^{-6}	8.6×10^{-8}
Paris	7,822	409	19,124	49°N	0.98	417	2.1×10^{-6}	3.4×10^{-8}
Shanghai	7,100	92	77,173	31°N	1.27	72	3.7×10^{-7}	5.9×10^{-9}
Chicago	6,805	947	7,185	42°N	1.10	861	4.4×10^{-6}	7.0×10^{-8}
Moscow	6,375	229	27,838	55°N	0.86	266	1.4×10^{-6}	2.2×10^{-8}
Calcutta	6,261	341	18,360	22°N	1.44	237	1.2×10^{-6}	1.9×10^{-8}
Bombay	4,871	81	60,135	19°N	1.51	54	2.7×10^{-7}	4.4×10^{-9}
Peking	4,200	117	35,897	39°N	1.14	103	5.2×10^{-7}	8.3×10^{-9}
Philadelphia	4,087	642	6,366	40°N	1.12	573	2.9×10^{-6}	4.7×10^{-8}

¹Twelve largest cities selected per 1966 National Geographic Atlas excluding Buenos Aires, for which P-95 data were not available.

²P-95 data from Bureau of the Census.

³Function of proportionate area in latitude range and impact probability in latitude range (SC-RR-66-41).

⁴Impact probability = $\frac{\text{effective area}}{\text{earth's surface area}}$.

⁵Impact probability = $\left(\frac{\text{effective area}}{\text{earth's surface area} = 1.97 \times 10^8 \text{ square miles}} \right) \times \left(\text{Probability of SNAP-19 getting} \right)$
in a short orbit = 0.016

[REDACTED]

SNAP-27

The SNAP-27 is a 56-watt thermoelectric power supply designed for lunar operating conditions. It will be used as the electrical power generator for the Apollo lunar surface experiment package (ALSEP). During the trip to the moon, the fuel capsule will be contained in a graphite LM fuel cask (GLFC); this is intended to protect the capsule during atmospheric reentry resulting from possible mission aborts. Final assembly of the SNAP-27 will be performed by astronauts on the lunar surface by inserting the fuel capsule into the generator assembly.

Maximum Pressure Coefficient on GLFC During Reentry (H. R. Spahr)

The maximum pressure coefficients during reentry for the GLFC were calculated at maximum convective heating and maximum deceleration for three different reentries. These maximum pressure coefficients, $C_{p \text{ max}}$, were based on an assumption of equilibrium flow. The results are:

<u>Trajectory Type</u>	<u>$C_{p \text{ max}}$ Maximum Heating</u>	<u>$C_{p \text{ max}}$ Maximum Deceleration</u>
Orbital decay	1.87	1.93
Shallow supercircular, $\alpha_E = -6.25^\circ$	1.93	1.94
Steep supercircular, $\alpha_E = -38.05^\circ$	1.92	1.93

This study confirms that the value of 1.93 being used by GE for structural loading is correct.

Radiant Heat Test (L. L. Keller)

A revised preliminary test plan was prepared and distributed. The revised plan incorporates the latest temperature versus time profiles calculated for a capsule in a graphite LM fuel cask exposed to (1) fireball/afterfire and (2) earth orbit decay environments.

~~CONFIDENTIAL~~

Calculation of Heating Rates to GLFC Ahead of Titanium Struts
(H. R. Spahr)

Heating rates to the GLFC ahead of the titanium struts were calculated for six flight conditions. The heating rate factors, in terms of stagnation heating to the GLFC cylinder, are:

- Orbital decay, maximum heating = 10.4.
- Orbital decay, maximum deceleration = 10.6.
- 6.4° supercircular reentry, maximum heating = 9.2.
- 6.4° supercircular reentry, maximum deceleration = 10.2.
- 38.05° supercircular reentry, maximum heating = 9.5.
- 38.05° supercircular reentry, maximum deceleration = 10.7.

The results of the analysis will be detailed in a report.

Spontaneous Ignition Temperature Studies (D. J. Sasmor/R. P. Wemple/
J. E. Boyd)

The determination of the effect of surfaces and gaseous environments on the ignition temperature of Aerozine 50 was continued this quarter.

Figure 2 shows the curves of the ignition temperature versus ignition times of Aerozine 50 in pyrex and graphite flasks in an air environment. The lowest ignition temperatures, i.e., the temperature below which no ignition occurs irrespective of time and volume of fuel used, are 266°C (510°F) in graphite and 270°C (518°F) in pyrex.

~~CONFIDENTIAL~~

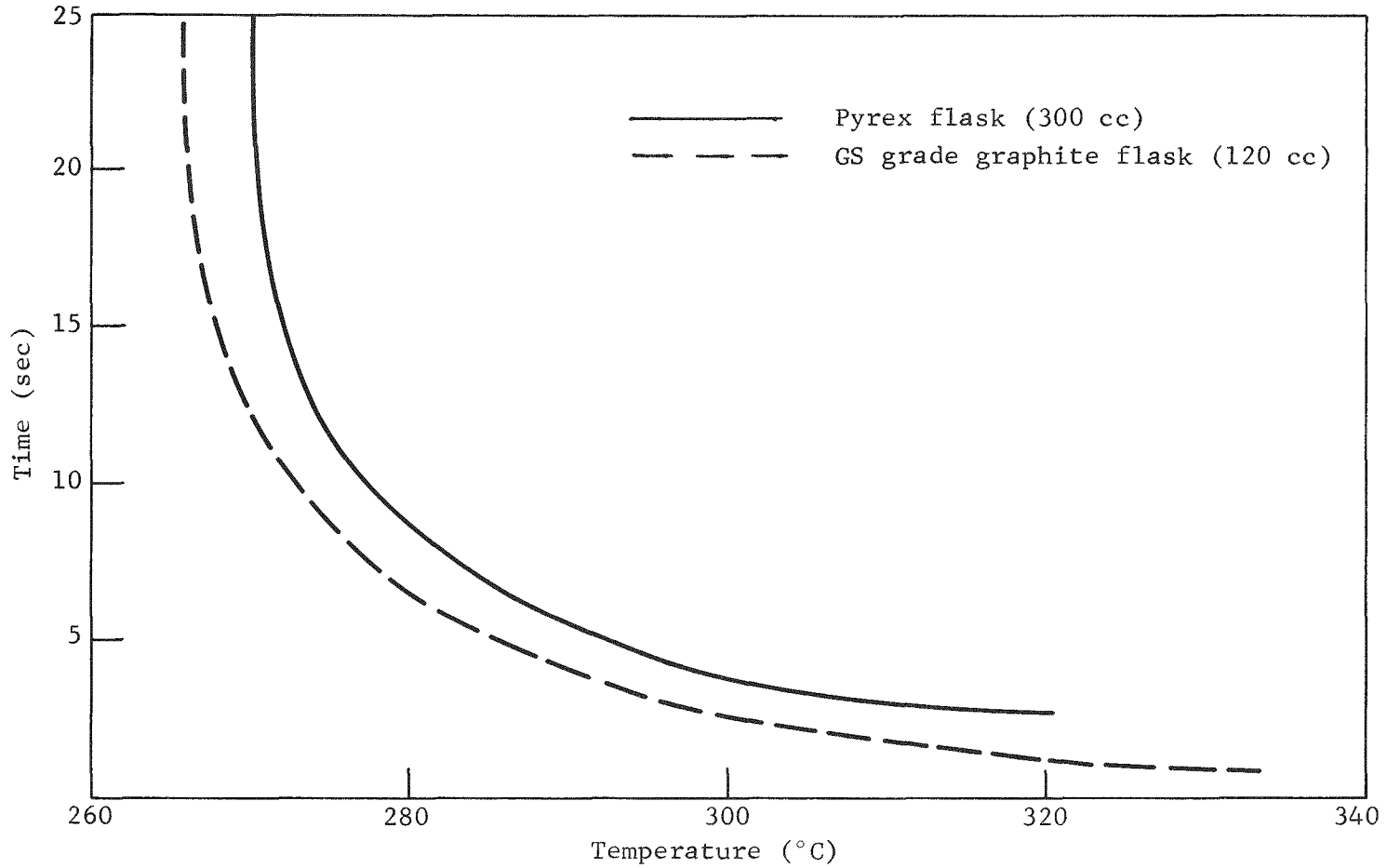



Figure 2. Spontaneous ignition temperatures versus average elapsed time to ignition in air for Aerozine 50 (D68-11027)



Complete curves as shown in Figure 2 were not developed for the ignition studies of Aerozine 50 in a nitrogen-oxygen ($5 \pm 0.5\%$) environment. These studies were limited to the determination of the lowest ignition temperatures. The oxygen concentration was monitored and adjusted using a Beckman E-2 Oxygen Analyzer. In addition, the gaseous environment was sampled randomly throughout the test series for mass spectral analysis. The oxygen concentration and range ($5 \pm 0.5\%$) are based on these analyses. The lowest ignition temperature for Aerozine 50 in graphite in a nitrogen-oxygen ($5 \pm 0.5\%$) atmosphere is 540°C (1004°F), and the lowest temperature for this system with a Hitco (pyrocarb 406) insert is 490°C (914°F).

The determination of the lowest ignition temperature of Aerozine 50 in graphite in a nitrogen atmosphere is incomplete. To date, no sharp cutoff or lowest temperature for ignition has been reached. In the high-temperature region (short ignition times) the curve appears normal (resembling Figure 2); however, as the temperature of the graphite flask is lowered, the time to ignition reaches a maximum of approximately 10 seconds and remains relatively constant in spite of continued lowering of the system temperature.

SNAP-27 Fire Model (G. H. Elkins)

Temperature versus time graphs were plotted using the data generated by preliminary mathematical models for different fire environments for the SNAP-27 generator. The following configurations were used in the model.

1. Cask and capsule in a residual fire.
2. Cask and capsule in a fireball.
3. Cask and capsule in both the fireball and residual fire.
4. Capsule in a residual fire.
5. Capsule in a fireball.
6. Capsule in both the fireball and residual fire.

The temperature versus time plots were constructed for the above configurations and situations. Figure 3 gives the outer fuel temperature for the SNAP-27 cask in a fireball plus residual fire. Figure 4 gives the outer fuel temperatures for the SNAP-27 capsule in a fireball plus residual fire.

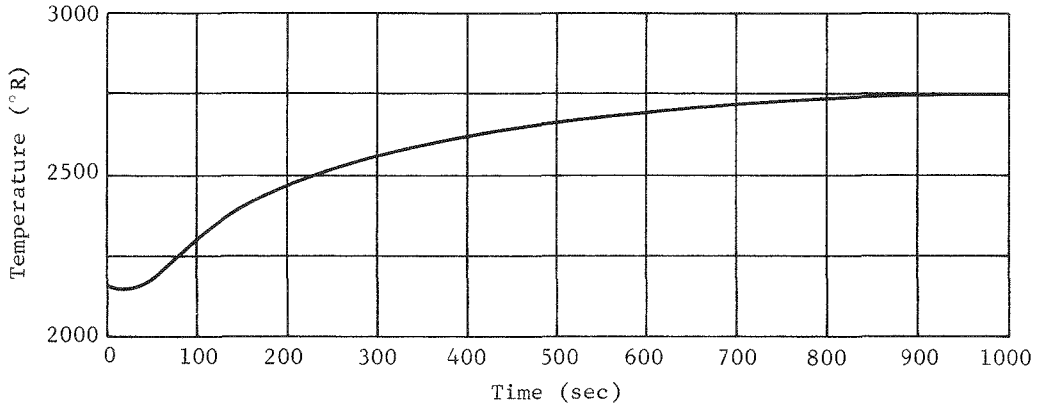


Figure 3. SNAP-27 cask in fireball and residual fire (D68-11028)

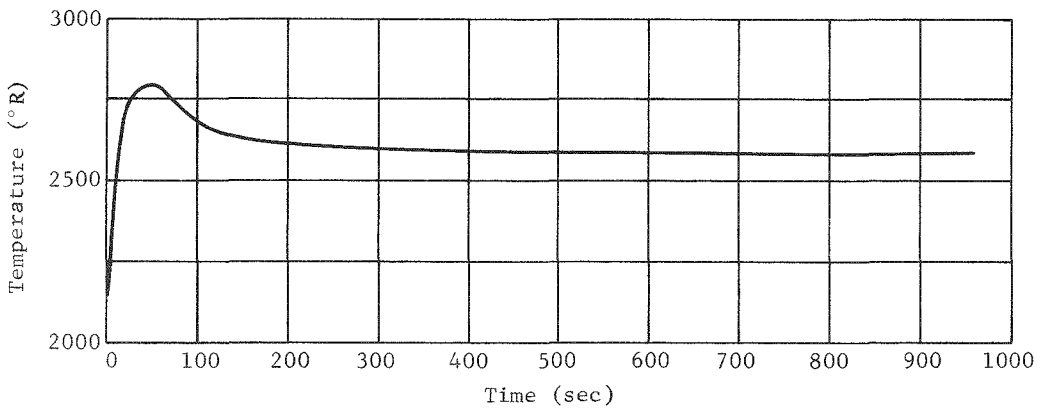


Figure 4. SNAP-27 capsule in fireball and residual fire (D68-11029)

~~CONFIDENTIAL~~

PLUTONIUM SYSTEMS SUPPORT


Analytical Study of the Hypersonic Reentry of Small Spherical Particles (B. W. Marshall)

During this period, work proceeded in defining a scope of work for a contract in the area of the reentry of small spheres. A three-phase overall program was outlined. A contract is presently being negotiated for Phase I of this overall plan. Essentially, this contract will require the contractor to: (1) examine a matrix of velocity/altitude release condition and place bounds on the important parameters occurring during reentry; (2) perform studies to estimate the relative importance of the parameters identified in (1); and (3) perform scaling studies to estimate the possible effects of altering parameters, as is required for laboratory experiments.

Stagnation Liquid Layer Ablation Study (B. W. Marshall)

Under Sandia contract, Cornell Aeronautical Laboratory (CAL) is developing a test facility for observing the behavior of spheres during melting ablation in hypersonic transition flow, with melting initiated at the stagnation point. The purpose of the experiments is to observe the loss of liquid particles from the main body of the sphere and, if it occurs, to observe the general disintegration of the sphere. The observations will be made over a range of Weber numbers from well below 6 to above 6, with some of the lower Weber number tests to be in transition flow. The influence of viscosity number on the behavior of the spheres will be explored.

A flow system is being developed in which a sphere will be supported in an essentially stable position by the drag force exerted by an upward test stream in a test chamber. Good photographic observation of the sphere during its melting ablation period will be possible. The rear section of each specimen will be distorted from the shape of a true sphere if this is required to prevent spinning. The materials of which the spheres will be made were selected after a literature study. The materials must meet certain requirements, such as desired values of melting point, surface tension, and viscosity. It is expected that the desired values can be obtained with metals, alloys, oxides, and



organics. Preliminary studies indicated that a system could be made to operate at a Mach number of 6 or above with spheres whose size will range from approximately 1 to 10 millimeters, with Weber numbers ranging from well below unity to well above 10; tests of the smaller spheres will be at Knudsen numbers near unity. The conditions are expected to be such that the melting cycle will require many seconds, probably a few minutes, for completion.

The initial work on materials for test spheres was confined, because of the previously stated requirements, to bismuth, tin-lead alloy, chromic anhydride, sodium-dichromate, lead bromide, and stearic acid. The materials to be used initially are bismuth and stearic acid, which present a range of viscosity of approximately 70 to 1. Spheres of bismuth were fabricated by casting in a boron nitride mold; stearic acid spheres were formed by an injection molding technique.

The flow system was designed, and drawings were transmitted for fabrication. Delivery of some of the larger sections of the flow system was delayed but has recently been accomplished. Assembly of the system for demonstration has started. This demonstration will consist of obtaining ablation data on the bismuth and stearic acid spheres.

Reentry Ablation Testing in a Hyperthermal Arc Tunnel (B. W. Marshall/
I. B. White/K. L. Romine)

Four $^{238}\text{PuO}_2$ microspheres coated with 40 to 45 microns of pyrocarbon were tested in the Sandia 40-kW hyperthermal arc tunnel. The purpose of the tests was to determine if carbon-coated microspheres would survive reentry heating for longer times than bare microspheres.

The first two tests were conducted at an enthalpy of 12,000 Btu/lb and a model pressure of 0.0987 atmosphere (Condition K). The 3000 fps films of these tests showed that the microsphere heated to a reasonably bright, hot condition with a uniform temperature across the microsphere. At approximately 0.050 second, the microsphere appeared to suddenly glow brighter and then disappear from the sting before the next film frame.

No motion of the microsphere prior to its disappearance could be detected. Small pieces of radioactive debris were found scattered about

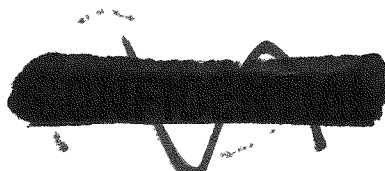
[REDACTED]

the test chamber. The vinyl-coated copper impact sampling plate, which was located 4 inches behind the microsphere, collected a large amount of debris. Autoradiographs of the sampler showed that the collected debris was in a random pattern (Figure 5). In all previous tests of microspheres with no carbon coating, the debris collected formed a symmetrical pattern which was concentrically located on the sampler. On the average, the debris from the carbon-coated microsphere was much larger than the debris from uncoated microspheres, and there was no evidence of the small, molecular-type of debris.



Figure 5. Autoradiograph of $^{238}\text{PuO}_2$ debris from pyrocarbon coated microsphere (D68-11030)

The third test, which was also conducted at Condition K, was unsuccessful because the microsphere fell from the sting approximately 0.010 second after exposure to the plasma stream. It is significant that the falling microsphere was observed in several frames of the movie film before it disappeared. This is typical of all previous tests in which the particle fell off the sting.



CONFIDENTIAL

The fourth test was conducted at Condition A which furnishes an enthalpy of 8000 Btu/lb and a model pressure of 0.0467 atmosphere. The sequence of events and the debris collected were the same as in the first two tests at Condition K, except that the time to sudden disappearance of the microsphere was 0.115 second. This time difference was caused by the lower heat flux of Condition A.

Based on the movie film, the debris scattered about the tunnel, and the debris collected on the sampler, it is hypothesized that the microspheres from Tests 1, 2, and 4 fragmented or exploded. The samplers from Tests 1 and 4 were sent to Tracerlab, Inc., for analysis of the collected debris.

Tests to determine the catalytic effects of $^{238}\text{PuO}_2$ were conducted in the Sandia 40-kW hyperthermal arc tunnel. Initially a 0.125-inch diameter flat-faced copper slug calorimeter was exposed to all the test environments presently being used. A similar calorimeter coated with approximately 1 micron of $^{238}\text{PuO}_2$ was exposed to these same conditions. A preliminary comparison of the results from the uncoated copper calorimeter and the $^{238}\text{PuO}_2$ -coated calorimeter indicates that there was an approximate 30-percent reduction in the heat flux to the $^{238}\text{PuO}_2$ -coated calorimeter.

A third copper calorimeter coated with SiO was also tested at these same reentry conditions. Since SiO is known to be noncatalytic, it will furnish a standard for comparison with the copper and PuO_2 -coated calorimeters. The data from the SiO-coated calorimeter have not been completely reduced at this time.

Three new tube assemblies were developed to hold the sting tips. The first holds the microsphere head-on in the plasma stream. To remove most of the tip and all of the tube assembly from the plasma stream, tube assemblies were developed to hold the microsphere at 45 and 90 degrees to the plasma flow axis. The tungsten tips used for the 45- and 90-degree positions were modified; a radius ground on the tip to match the radius of a 220-micron particle will help hold the particle in the stream.

CONFIDENTIAL

CONFIDENTIAL

Analysis of Debris from Ablation of $^{238}\text{PuO}_2$ Microspheres in a Hyperthermal Arc Tunnel (I. B. White/J. F. Hudson)

The debris ablated from $^{238}\text{PuO}_2$ microspheres in the Sandia 40-kW hyperthermal arc tunnel are being analyzed by Tracerlab-West, Inc. Previously, the method of analysis was essentially as follows.

1. The debris was removed from the impact collection sampler by dissolving the vinyl coating containing the particulate from the sampler.
2. The solution was centrifuged, and the excess solution was removed.
3. The remaining solution was transferred to microscope slides, and a size distribution analysis was performed by the hollow star method of sizing radioactive particles.

The resulting size distribution of this analysis for particle M-35, ranged from 0.1- to 1.6-micron diameter, with the peak occurring at approximately 0.2 micron. However, a radioactive count of the sized particles showed that they represented only a small portion of the total mass collected.

In order to determine the location of the remaining mass of $^{238}\text{PuO}_2$, a radiochemical mass balance was conducted on sampler M-35. The reentry test condition for microsphere M-35 was K (enthalpy 12,000 Btu/lb, model pressure 0.0987 atmosphere). This sampler had been previously analyzed by the method described above. The mass balance included the centrifuged residue, the centrifuged supernate, the impact sampler, and the particles previously analyzed for size distribution. The size distribution resulting from the radiochemical analysis is significantly different from that previously reported in that 95.79 percent of the mass is comprised of particles less than 0.05 micron diameter. The majority of the mass was located in the centrifuged residue. Since the lower limit for determining the sizes of particles is currently 0.05 micron, no size distribution could be made for the mass of $^{238}\text{PuO}_2$ less than 0.05-micron diameter.

This same complete radiochemical mass balance was conducted on two additional impact samplers. The two reentry environments represented by these samplers are Condition M (enthalpy 10,000 Btu/lb, model

CONFIDENTIAL

[REDACTED]

pressure 0.204 atmosphere) and Condition A (enthalpy 8000 Btu/lb, model pressure 0.0467 atmosphere). Table XII shows the size distribution of all the debris from samplers M-35, M-29 and M-3.

TABLE XII
 Percentages of Total Mass Versus Size Ranges
 of $^{238}\text{PuO}_2$ Debris Particles from Microspheres
 Tested in Hyperthermal Arc Tunnel
 (D68-11031)

Size Range of Particle Diameters (μ)	Equivalent $^{238}\text{PuO}_2$ Mass (μg)	Percent	Cumulative Percent
<u>Sampler M-35 (Condition K)</u>			
0 - 0.05	0.3390	95.79	95.79
0.05 - 0.10	0.0122	3.45	99.24
0.1 - 1.6	0.0027	0.76	100.00
<u>Sampler M-29 (Condition M)*</u>			
0 - 0.2	1.649	95.1	95.1
0.2 - 14	0.084	4.9	100.0
<u>Sampler M-3 (Condition A)</u>			
0 - 0.3	0.071	99.86	99.86
0.3 - 0.9	0.098×10^{-3}	0.14	100.00
<p>*The total amount of plutonium found on this impactor by radiochemical analysis and particle studies is 2.6 percent of the mass of the particle before ablation. This amount as determined by γ-counting the impactor after exposure is 0.97 percent of the mass of the particle before ablation.</p>			

Since only a small percent of the total ablated mass was collected and analyzed, Table XII is not an absolute indication of the size distribution for the entire ablated mass of $^{238}\text{PuO}_2$. A theoretical mass balance analysis of the total ablated debris is currently being conducted. This analysis includes flow patterns, sampler efficiency, and data recorded on the movie films. Results will be published when the analysis is completed.

[REDACTED]

Gas Gun Tests (B. W. Marshall)

Under Sandia contract, ACDRL conducted eight experiments using Al_2O_3 microspheres and seven experiments using gold microspheres in the ACDRL light gas gun. The results of the alumina experiments were reported previously. The alumina experiments were not completely successful because no laser shadowgraphs were obtained due to failure of the triggering systems.

Calculations comparing the melt response of Al_2O_3 and gold microspheres in the ACDRL 120-foot range were performed. These calculations showed that for conditions of interest and within the available 120-foot range, insufficient melting of the Al_2O_3 occurs to permit reliable detection on the laser photographs. Curves showing the melt response of 400-micron diameter gold, alumina, and fuel material are shown in Figure 6. Based on these calculations, it was decided at a meeting held at Sandia with Martin, ACDRL, Sandia Isotopic Projects, and Sandia ANS personnel in attendance, that the initial shots in the remaining portion of the study would be done using gold microspheres. If other materials then appear feasible, they will be considered later.

Based on the unsuccessful results of the experiments using alumina particles, ACDRL personnel modified the laser photograph trigger system to obtain more reliability. Following these modifications, seven additional shots using gold microspheres were completed. These experiments were considered successful in that laser photographs and good impact data were obtained. Table XIII presents the limited data presently available on these experiments.

On the 7 shots completed using gold particles, a microwave trigger system for one laser was used with excellent reliability. Sandia has granted a delay in testing until January 1968 for the remaining 15 shots based on ACDRL providing at least two and more likely three microwave trigger systems for the remainder of the program.

Fifteen shots remain to be performed under this contract. A conference between Sandia and ACDRL personnel was held to provide direction for these remaining shots. ACDRL personnel were advised that the goal for this program is to reduce the flight Weber number as much as possible and still retain liquid layer melting.

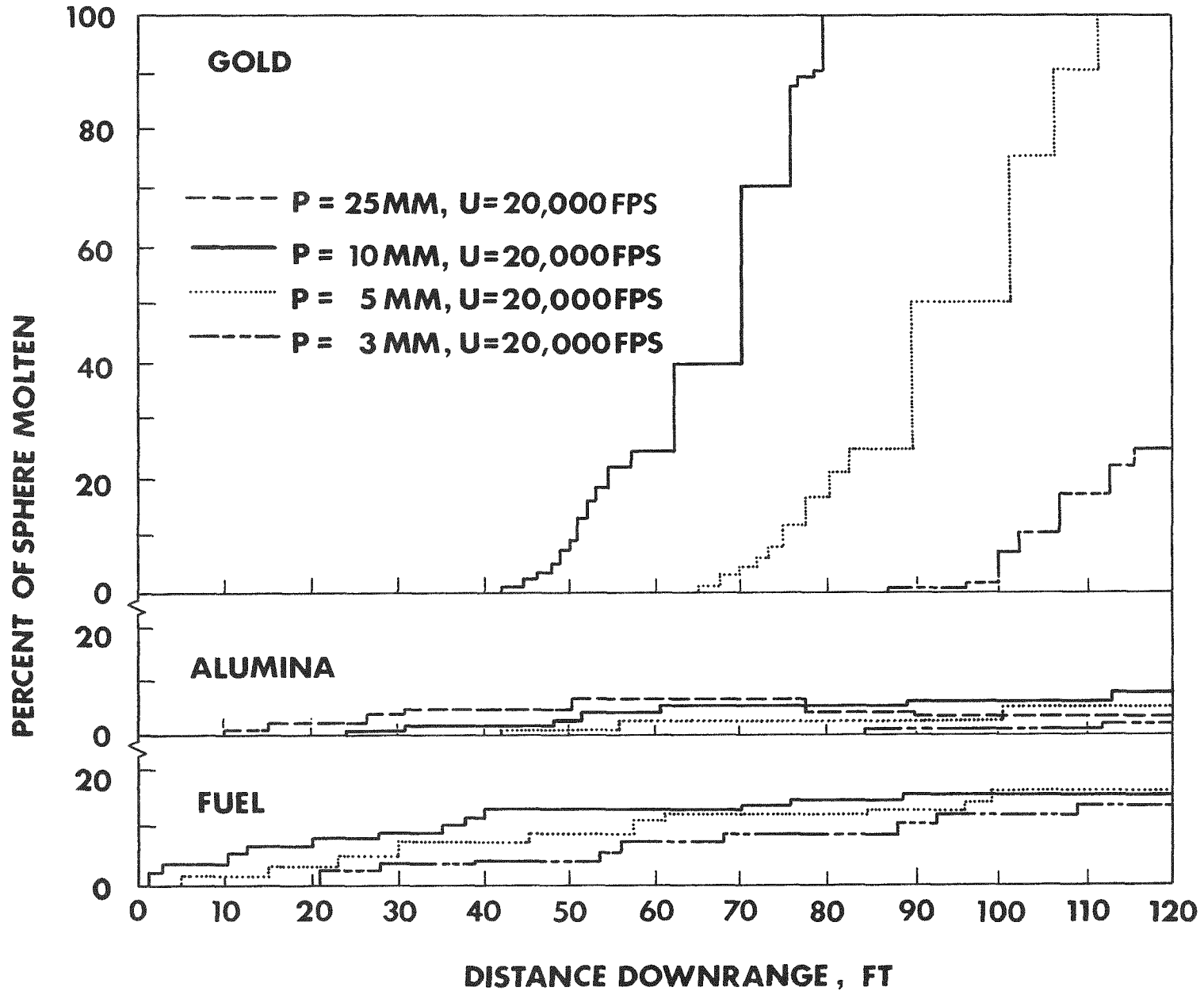


Figure 6. Comparison of melt response for free-flight gun range (D67-15696)

~~CONFIDENTIAL~~

TABLE XIII

Results of Gas Gun Tests Using Gold Microspheres
(D68-11032)

<u>Shot</u>	<u>Nominal Diameter (microns)</u>	<u>Range Pressure (torr)</u>	<u>Velocity (fps)</u>	<u>Comments</u>
G-1	620	8	21,900	Laser photograph shows melt and ablation.
G-2	620	8	21,900	Laser photograph shows melt and ablation.
G-3	520	7	21,900	Laser photograph shows melt and ablation.
G-4	520	7	21,900	Laser photograph shows melt and ablation.
G-5	520	2	21,900	Single impact crater; no melt apparent.
G-6	380	7	21,900	No laser photographs; impact shows fine debris.
G-7	380	2	21,900	Large impact and several smaller ones on plate.

ACDRL personnel recently suggested some possible firing conditions for the 15 remaining shots. The conditions were selected to provide a partially molten particle in the flight chamber at the minimum Weber numbers compatible with range limitations. For these conditions, a fast acting valve will be placed 20 feet downrange from the gun nozzle. This initial 20-foot section will be at a relatively high pressure such that the particle will enter the 100-foot chamber at 1 torr pressure through the fast acting valve at a temperature somewhat below melting. Final heating, melting, and ablation will occur in the low pressure, low Weber number range. The suggested conditions are shown in Table XIV. Sandia calculations to check the ACDRL calculated melt initiation locations are under way but are incomplete at this time.

Sandia fabricated and shipped samplers to ACDRL for use in an attempt to obtain debris from the microsphere as it ablates down the range. The samplers consist of 1-foot long, 4-inch-diameter cylinders with end caps in which 1.5-inch-diameter holes were drilled. The inside of each

~~CONFIDENTIAL~~

[REDACTED]

cylinder is lined with IPC filter paper which is changed for each run. The principle of operation for these samplers is that the original microsphere will pass through the holes in the cylinder and some of the debris generated will be removed from the wake and be trapped on the filter paper. These samplers will be placed along the range ahead of the impact plate, and attempts will be made to analyze the gold debris using neutron activation techniques.

TABLE XIV

Typical Firing Conditions Suggested
by ACDRL for Remaining Gas Gun Shots
(D68-11033)

Size (μ)	Velocity (ft/sec)	20-Foot Section			80-Foot Section		
		Pressure (mmHg)	Temperature Rise ($^{\circ}$ R)	Exit Velocity (ft/sec)	Pressure (mmHg)	Start Melt (ft)	Weber Number, (W)
200	12,000	8	560 - 1380	11,830	1	91	2.19
200	12,000	1	560 - 850	11,975	1	127	2.24
200	14,000	3	560 - 1280	13,920	1	75	3.04
200	14,000	1	560 - 960	13,975	1	90	3.06
250	14,000	8	560 - 1380	13,840	1	90	3.76
250	14,000	1	560 - 840	13,980	1	130	3.84
250	16,000	3	560 - 1250	15,930	1	78	4.97
250	16,000	1	560 - 950	15,975	1	93	5.00

$$W = \frac{\rho_{\infty} U_{\infty}^2 r}{\sigma}, \text{ where } \sigma = 1000 \text{ dynes/cm.}$$

40-kW Arc Jet Sampler (R. E. Smith)

The design feasibility of a new combination impactor-filter sampler for the 40-kW arc jet was studied. Preliminary calculations indicate that if the IPC filter paper can be shielded from the direct radiant heat of the arc during the test period, the gas, after it flows past the first stage impactor collection plate and the following shield zone, may not be hot enough to burn the filter paper.

If the filter paper is not destroyed, the collection efficiency of the new sampler should be much higher than the present impact sampler, and the data reduced from the collected sample should be more

[REDACTED]

representative of the true particle size distribution formed during the microsphere ablation tests. If the paper is destroyed during the preliminary checkout tests, an attempt will be made to cool the gas prior to discharge through the filter paper.

Formation of Plutonium Carbide (D. J. Sasmor)

One of the hazards postulated regarding the SNAP-27 graphite cask and fuel capsule is the intact burial and subsequent encapsulation in a nonpermeable cocoon. In this situation, we postulate that the plutonia fuel is in contact with the graphite of the cask. If this does occur, how much plutonia will react with the cask material to form plutonium carbide?

Under the conditions stated, i.e., sealed cocoon, no gas enters or escapes; therefore, the quantity of plutonia that reacts with the graphite depends on the equilibrium pressure of carbon monoxide. The net reaction to form Pu_2C_3 from PuO_2 , neglecting the mechanisms, is



Utilizing free energy data, the equilibrium pressure for the carbon monoxide can be calculated, and assuming an internal void volume of 10 liters we can calculate the amount of $\text{PuC}_{1.5}$ formed.

<u>T° C</u>	<u>Gram $\text{PuC}_{1.5}$</u>
1500	~ 0.12
2000	~ 4.4

Release of Gases from PuO_2 (C. J. Northrup/R. E. Berry)

Recent experiments at Mound Laboratory indicate that a large percentage of the helium generated by the alpha decay in $^{238}\text{PuO}_2$ is retained in the lattice structure. Subsequently, questions as to the possible sudden release of this gas have been posed. The fraction of the gas which is released during a particular time interval is a function of the diffusion coefficient of the material and the effective

~~CONFIDENTIAL~~

radius of the particle. At different temperatures, different processes predominate in the release of the helium; therefore, to be able to predict the rate of release of the helium requires knowledge of the diffusion coefficient as a function of temperature and the concentration of helium in the fuel. The effective radius of a particle is a sensitive function of the ratio of actual density to the theoretical density due to the increased surface area. For example, in UO_2 which has some physical properties similar to PuO_2 , if the actual density is 83 percent of the theoretical density the effective radius can be reduced by a factor of 10,000.

Experiments at Mound and LASL indicate the gas retention and release can be explained by diffusion theory. Fick's law states that the flux, J , of atoms passing through a surface is proportional to their concentration gradient:

$$J = -D \frac{\partial C}{\partial X},$$

where D is the diffusion coefficient, C is the concentration, and X is the distance. Since helium is being generated throughout the microsphere, an additional source term must be added. Therefore, the equation expressed in spherical coordinates which describes the processes is

$$\frac{\partial C}{\partial t} = D \left(\frac{\partial^2 C}{\partial r^2} + \frac{2}{r} \frac{\partial C}{\partial r} \right) + B e^{-bt},$$

where t is time, r is the radius, and B is the product of the decay constant b and the initial number of atoms of ^{238}Pu per cc. An algebraic solution to this problem was obtained:

$$C = C_s + e^{-bt} \left(\frac{-B}{b} + \frac{B}{b} \frac{a}{\sin a \sqrt{b/D}} \cdot \frac{\sin r \sqrt{b/D}}{r} \right) + \sum_{n=1}^{\infty} A_n \frac{\sin h_n r/a}{r} e^{-h_n^2 \pi^2 D t/a^2},$$

~~CONFIDENTIAL~~



where

$$A_n = \frac{-2(-1)^n a}{n\pi} \left(\frac{B}{b - n^2(\pi^2 D/n^2)} - C_s \right).$$

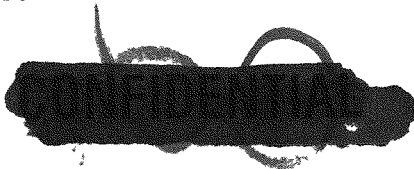
Here, a is the effective radius of the microsphere (the geometric radius compensated for porosity) and C_s is the saturation concentration determined by the partial pressure in the ambient atmosphere. Additional solutions were obtained for

$$\frac{\partial C(r)}{\partial t} \text{ and } \frac{\partial C(t)}{\partial r}.$$

In addition to the algebraic solutions, finite difference solutions were obtained which give answers which are consistent with the algebraic expressions. Both solutions have been programmed for computer analysis. These analyses give the concentration and rate of change of the concentration with respect to time at seventy points on the radius at selected instants in the lifetime of the particle. Simultaneously, the instantaneous flow rate through the surface, the instantaneous generation rate, and the total quantity of helium generated up to the selected instant are printed.

Figures 7 and 8 show examples of solutions obtained for the helium release rates and generation rates for microspheres with a diameter of 150 microns and a diffusion coefficient of $3.97 \times 10^{-15} \text{ cm}^2/\text{sec}$. The release rate equals the generation rate in 80 to 100 years for these conditions. The concentration of helium as a function of radial distance is shown for these conditions in Figure 9. Figure 10 indicates the effect of a sudden temperature rise. When the temperature (diffusion coefficient) is suddenly increased, the release rate of the gas increases and may persist above the generation rate for an appreciable time. Figures 7 through 10 were not corrected for the increased surface area due to porosity and are based upon a perfectly fused microsphere. Each curve represents the concentration at some specific time (years).

Figures 11 and 12 allow one to calculate the fraction of gas released as a function of the diffusion coefficient and particle size. Plans are under way to determine how the diffusion coefficient varies with temperature and time.



CONFIDENTIAL

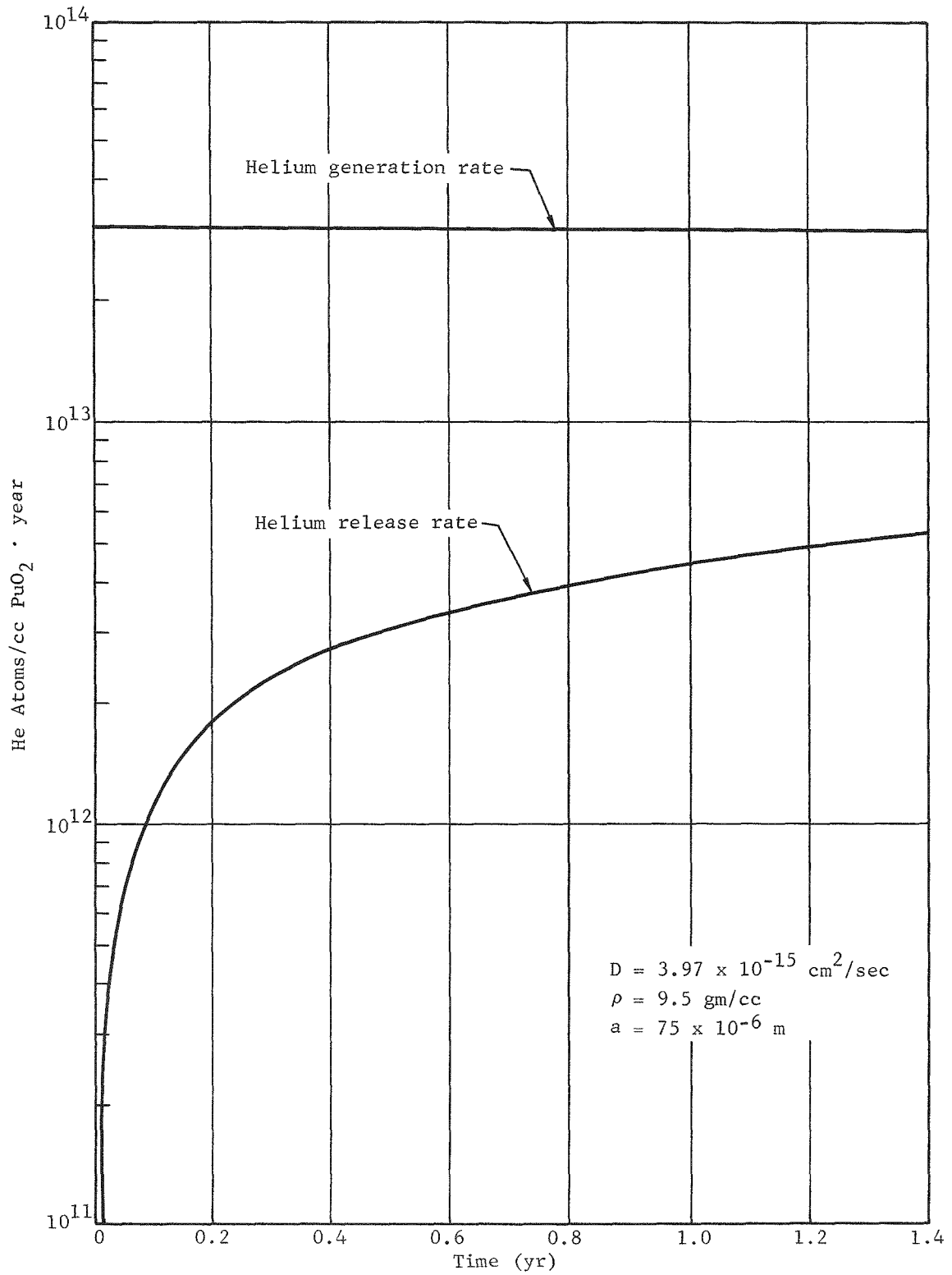


Figure 7. Helium release rate (D68-11034)

CONFIDENTIAL

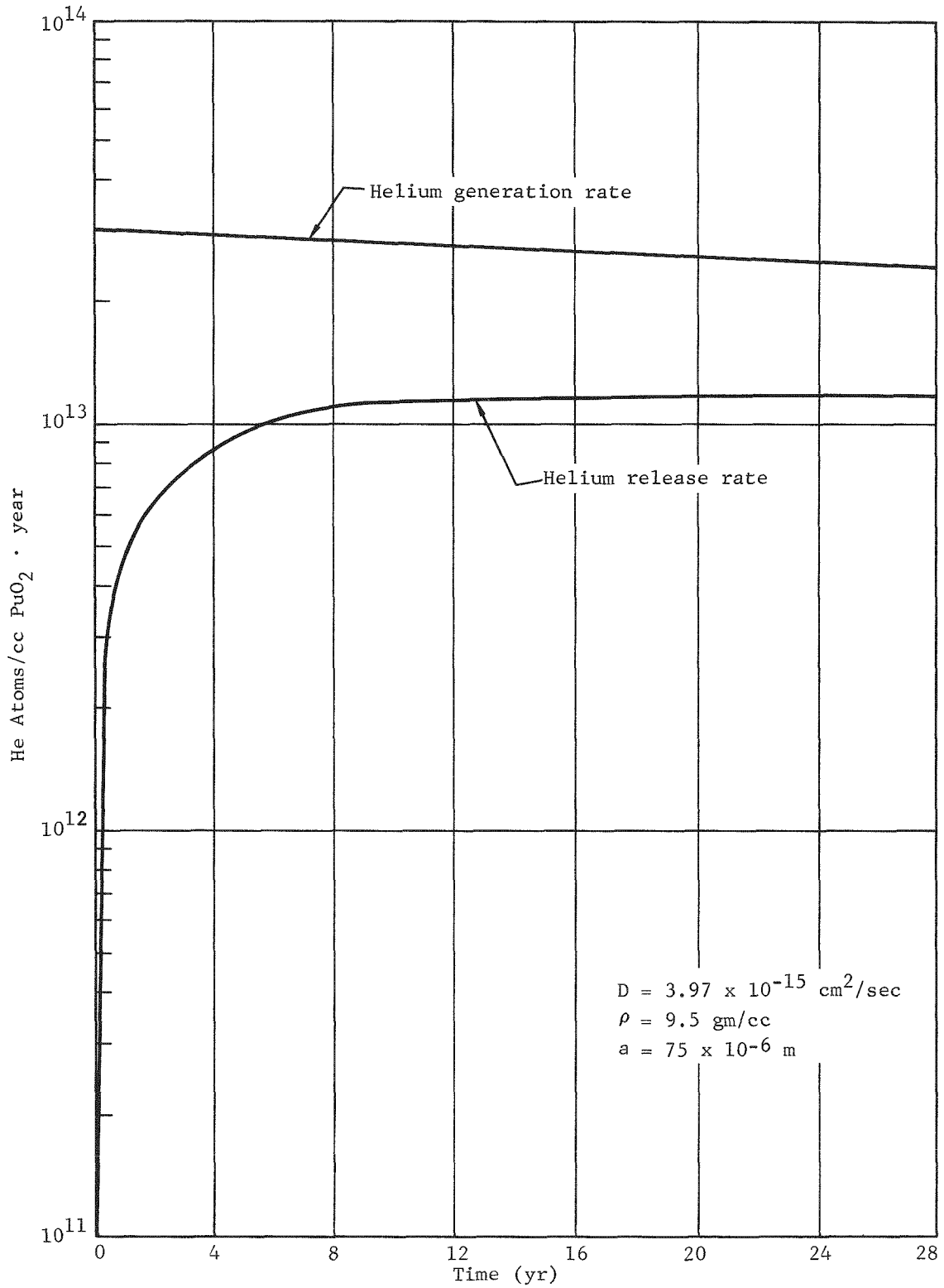


Figure 8. Helium release rate (D68-11035)

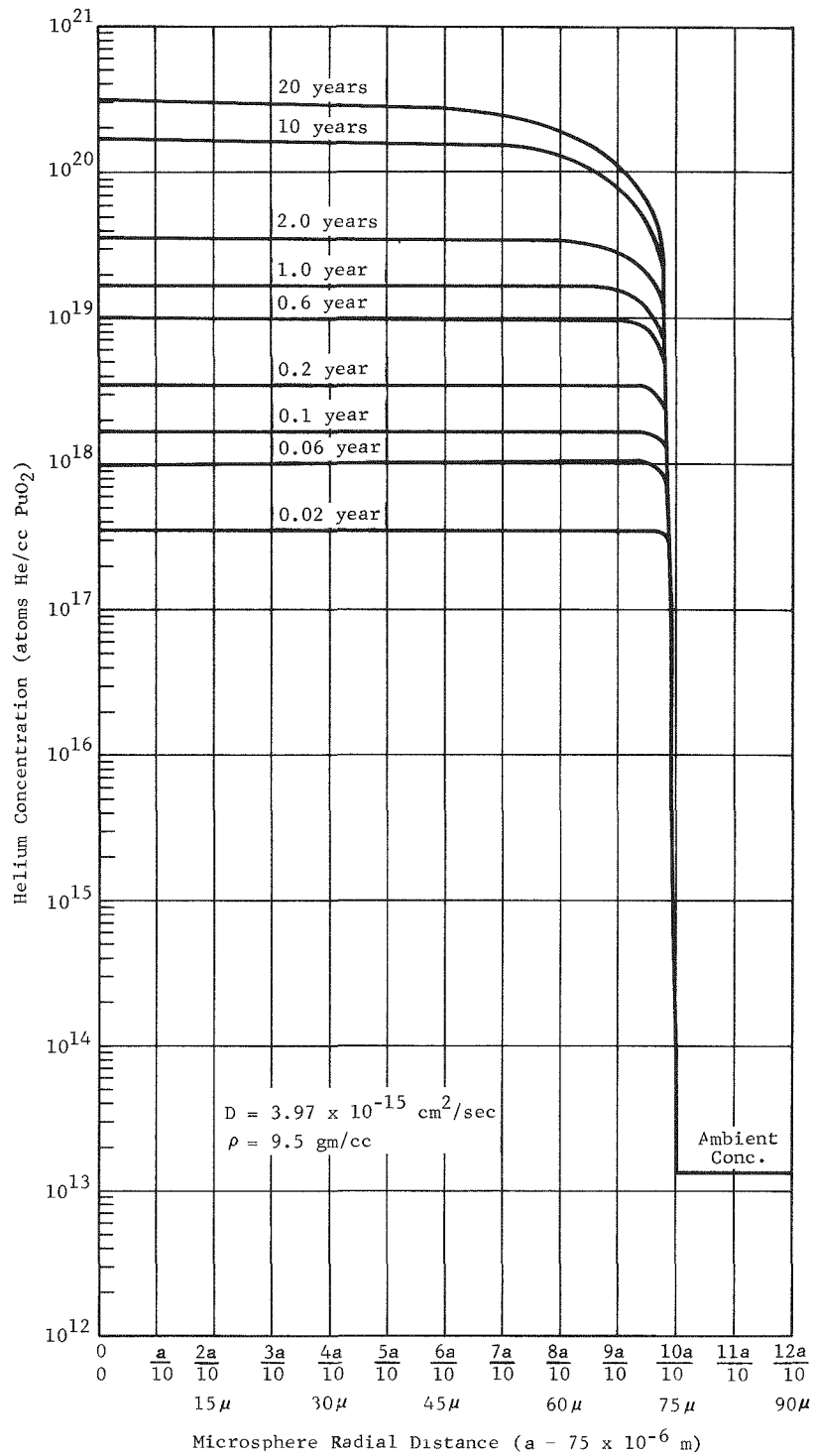


Figure 9. Concentration of helium as a function of radial distance (D68-11036)

CONFIDENTIAL

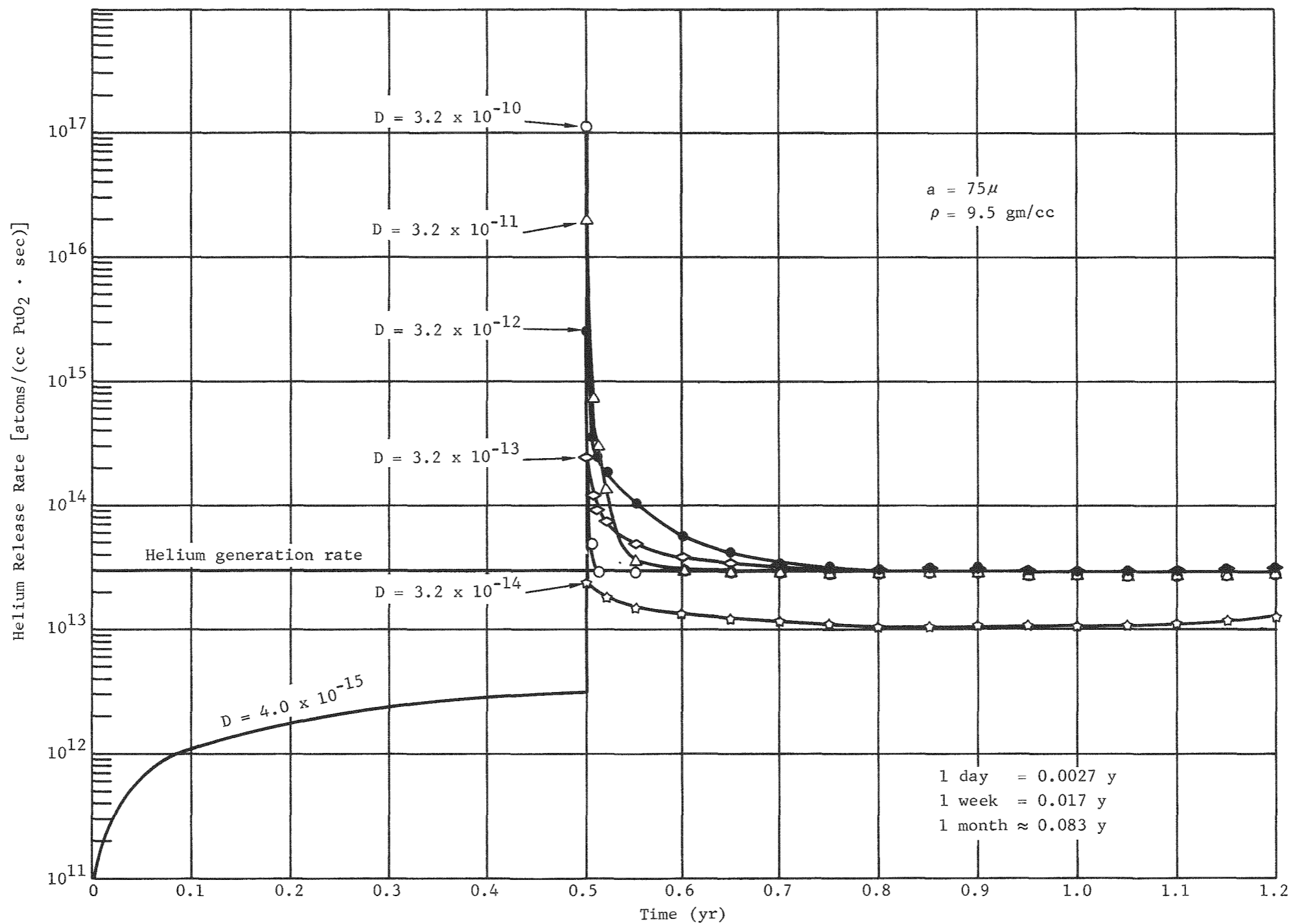


Figure 10. Helium release rate as a function of time (D68-11037)

CONFIDENTIAL

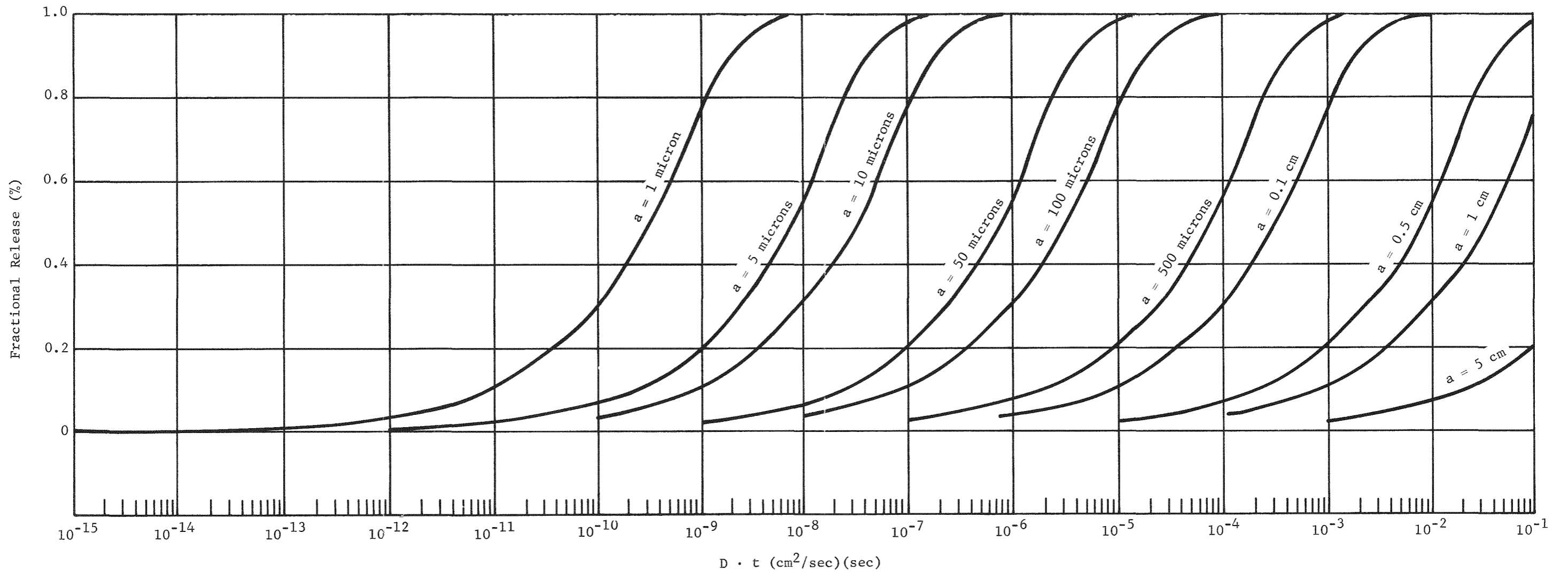


Figure 11. Fractional release versus (diffusion coefficient)(time) for various radii of microspheres (D68-11038)

CONFIDENTIAL

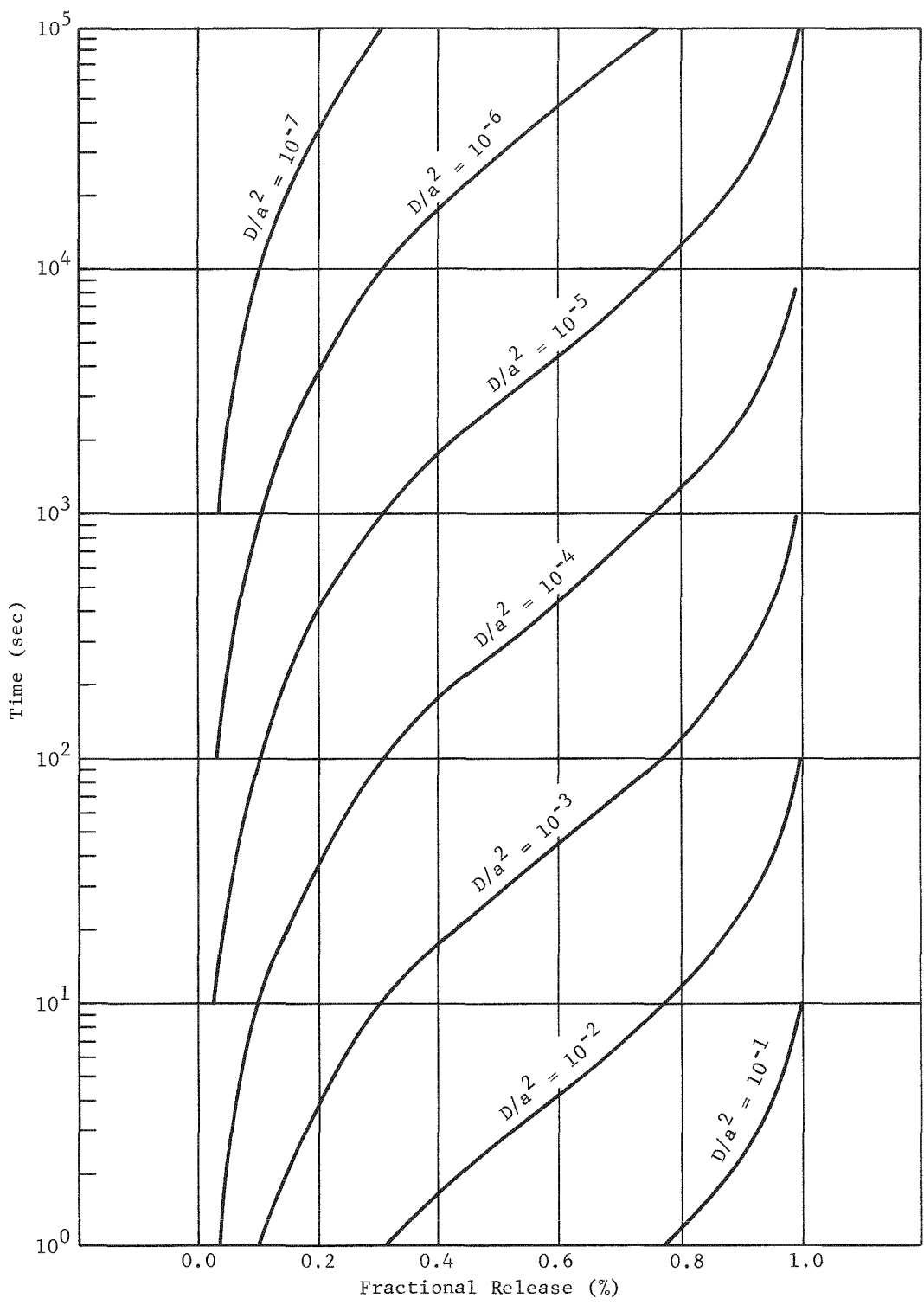


Figure 12. Fractional release versus time for various (diffusion coefficient)/(microsphere radii) (D68-11039)

CONFIDENTIAL

[REDACTED]

Radiation damage has a tendency to reduce the diffusion coefficient. The creation of microvoids impedes the motion of the helium; however, when the microvoids move to the surface, much larger fractions of stored helium may be released in bursts. Microvoid migration is a high-temperature phenomenon and has been reported in UO_2 at 1500°C .

Reducing the temperature has also been observed to contribute to the release of gases in UO_2 . Sudden temperature reductions may cause spalling and fracturing. This increases the surface-to-volume ratio, and fractures may release helium from microvoids, closed pores, or voids.

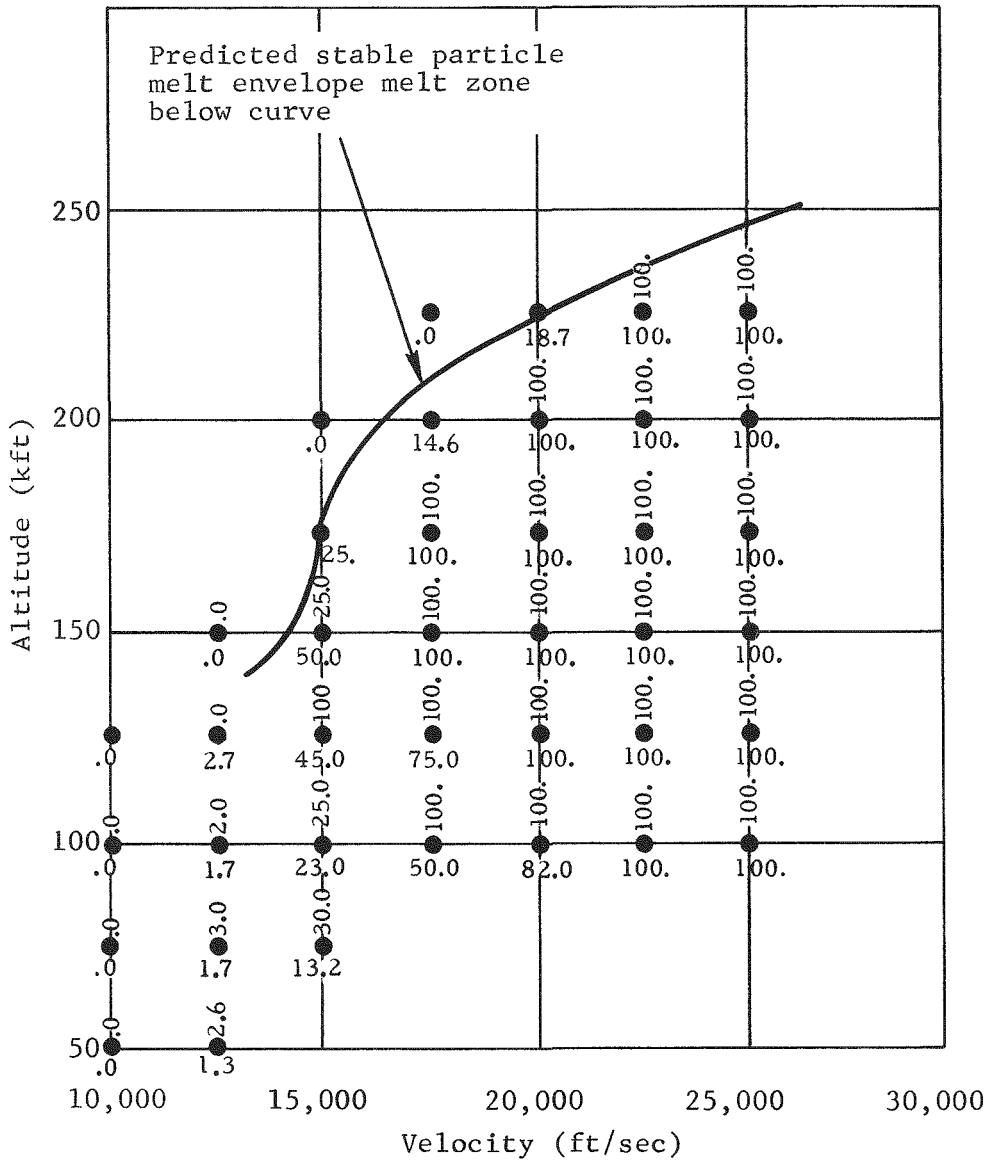
Surface absorption also will account for a significant release of gas when the temperature is raised from an initial low value. The use of many small particles results in a large surface area and numerous sites for gas adsorption.

Experiments are being conducted at both Mound and LASL to identify the mechanisms for gas release, and to determine the actual rates of generation of free gas which might be expected from PuO_2 .

Melt Matrix Calculations (C. B. Watkins)

The maximum percentages of melt which occur for fuel particles under various release conditions were calculated. The particle sizes investigated were 250 and 50 μ . The results are shown in Figure 13.

A curve of constant percentage melt for a fixed particle size would "bend back," i.e., tend toward increasing velocity at the lower altitudes. The melt envelope itself will not exhibit this trend. It should approach some near vertical asymptote of approximately 12,000 fps. This behavior is illustrated by the approximate curves of constant percentage melt for a 250- μ particle shown in Figure 14. Similar curves for a 50- μ particle would be shifted to the left and would be spaced somewhat closer together. It should be noted from Figure 14 that slight adjustment may be warranted in the previously published particle melt envelope (see Figure 13). The curves in Figure 14, however, are only approximate and result from interpolation between matrix points shown in Figure 13. In calculating the percentage melt, it was assumed that the particles always remained spherical.



Vertical figures are % melt of 50- μ particles.
 Horizontal figures are % melt of 250- μ particles.

Figure 13. Maximum percentages of melt for fuel particles under various release conditions (D68-11040)



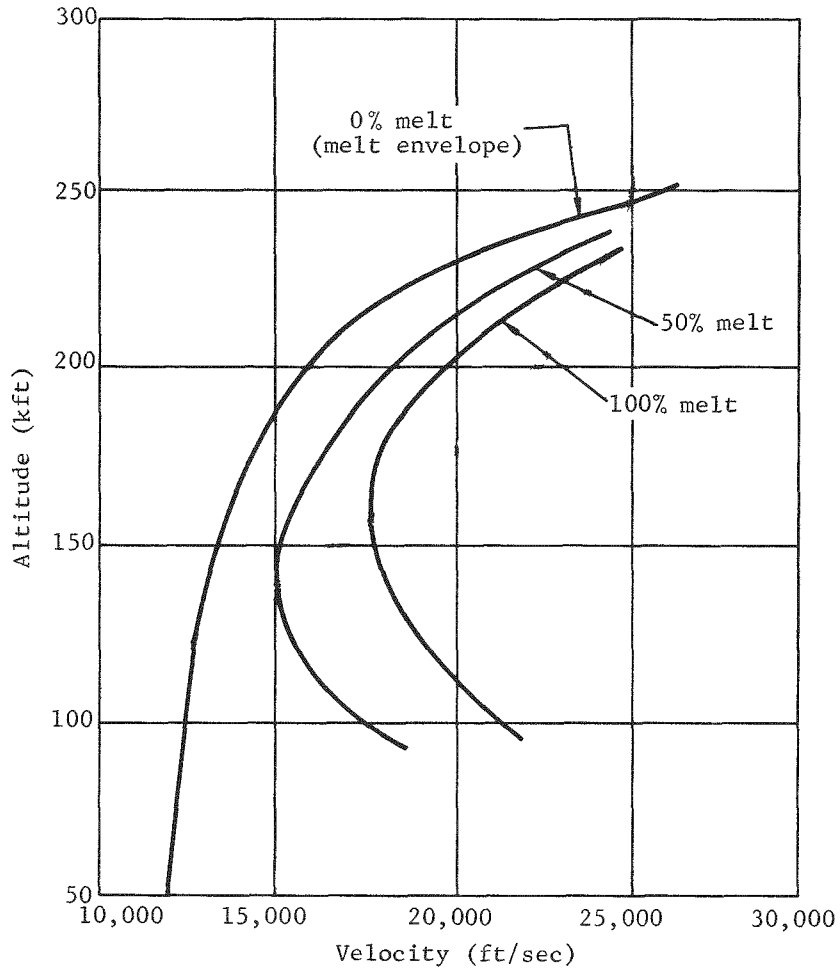


Figure 14. Constant percentage melt for a 250- μ fuel particle (D68-11041)

Fuel Simulant Studies (B. S. Hill)

The filling of three impact capsules with 32- to 128-micron plasma-fired zirconium dioxide microspheres was completed. These microspheres are closer to the size range of the actual fuel than were the microspheres used in previous tests. The capsules will be heated to 1000°F and impacted into granite, concrete, and earth targets at 100 fps. Fines analyses of this material will be performed to determine if there is a correlation in an impact environment between this prospective fuel simulant and PuO₂.

Fuel Fines from Impact (B. S. Hill)

Data from a Tracerlab fuel analysis (performed for Mound Laboratory) were extended in an effort to provide a useful tool for predicting fuel fines in a system analysis. The analysis was performed on fuel fines derived for an impact test performed at Sandia. Production grade fuel (SNAP-19/SNAP-27) was enclosed in a rigid capsule, heated to 1000°F, and impacted into granite at 105.9 ft/sec. Subsequently, Mound analyzed the fuel and determined that 0.025 percent by weight was less than 10 microns in size. A representative sample of the fuel particles less than 10 microns was selected by Tracerlab and sized. Figure 15 illustrates the distribution of particles by size. There is no explanation for the apparent lack of particles in the 2 to 10-micron range; however, some of the possibilities are: (1) characteristic breakup of the fuel particles, or (2) particle screening by Mound or Tracerlab. At present there is insufficient information to establish a confidence level for the distribution illustrated.

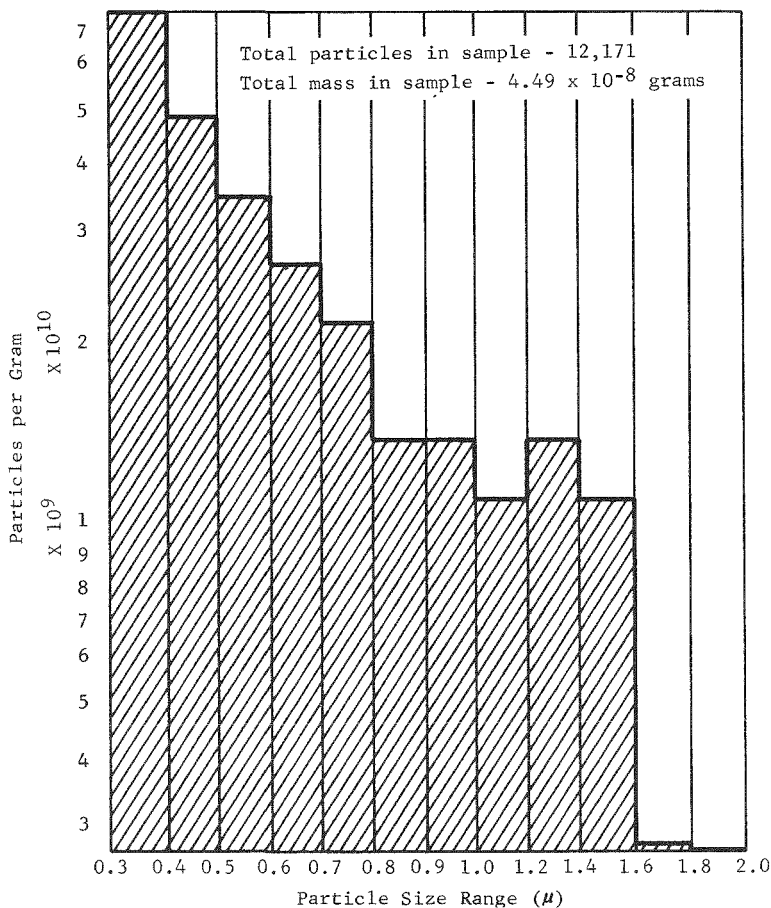


Figure 15. Particles per gram of PuO₂ (<10 μ) after 105.9 fps granite impact (D68-11042)

[REDACTED]

One live fueled impact capsule was heated to 1000°F and impacted at 116 fps into a concrete target at the Sandia Lunar Beam facility. The capsule was returned to Mound Laboratory for analysis.

Tracerlab-West, Richmond, California, will conduct fines analyses on representative samples in the under 20-micron range. Their first analysis will be performed on a sample from the above test.

Solubility Studies (W. L. Holley)

Under Sandia contract, ORNL developed and calibrated equipment that will be used to determine the solubility rate of $^{238}\text{PuO}_2$ fines in simulated lung fluid* and water. Progress on this work is as follows.

1. In order to establish correction factors for the self-absorption of the alpha particles by salts in the simulated lung fluid, samples of fluid containing known amounts of ^{239}Pu were evaporated on planchets, and the residual radioactivity was counted. In addition, a trial run was made using soluble plutonium-239 nitrate $[\text{Pu}(\text{NO}_3)_4]$ in 0.1 N HNO_3 to determine the equilibrium rate through the semipermeable membrane. It was found that the cellulose acetate used as the semipermeable membrane is an ion complexer which attracts plutonium ions and therefore gives incorrect results. This problem was alleviated by using an animal tissue membrane.
2. Figure 16 is an electron micrograph of $^{238}\text{PuO}_2$ fines produced by ORNL sol-gel. The larger particles are approximately 0.3μ in diameter, and the smaller ones are on the order of 50\AA in diameter.
3. Production $^{238}\text{PuO}_2$ fines are being obtained from Mound Laboratory. It is thought that solubility data from this type of experiment will be available as input data to the overall inhalation model within the next few months.

*Gamble, G. L., Chemical Anatomy, Physiology, and Pathology of Extracellular Fluid, A Lecture Syllabus; Harvard University Press, Cambridge, Massachusetts (1952).

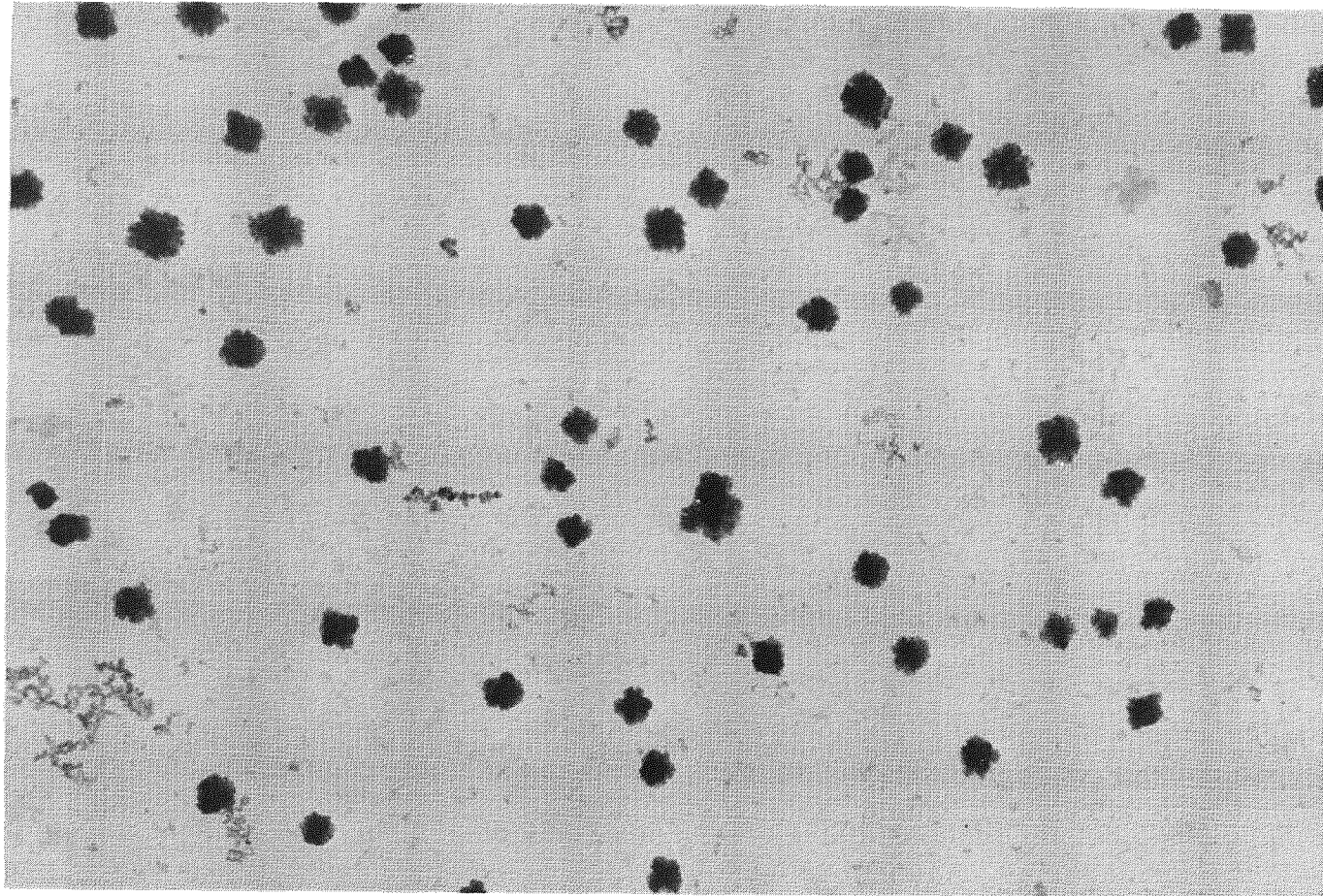


Figure 16. Electron micrograph of $^{238}\text{PuO}_2$ (24,000X)
(D68-11043)

CONFIDENTIAL

Correlation of Reported Plutonium Surface Air Concentrations with Measured Lung Burdens (R. J. Everett/W. D. Burnett)

A study was recently completed which reviewed the reported plutonium surface air concentrations and the measured amounts of plutonium in human lungs.* The reported air concentrations from 1955 to August 1966 were put through an inhalation model, recently computerized from the ICRP Lung Dynamics Committee's recommendations, in order to predict the amounts of plutonium expected to be in the lungs of the general population. Using five integration periods corresponding to the average plutonium concentration reported for that time period, the amounts predicted as of August 1966 were 3.16×10^{-13} curies. This value compares with the average measured lung burden by tissue assay of 4.4×10^{-13} curies. It appears that the use of the new lung model and the reported surface air concentrations will allow one to predict the lung burden in the general population with good accuracy.

Inhalation Studies (W. L. Holley)

In order to assess the hazards of inhaled $^{238}\text{PuO}_2$ or any other fuel, it is necessary to know the inhalation efficiency of various particle sizes and densities. For experimental determinations, ORNL, under Sandia contract, designed a pump which simulates to an acceptable degree the action of the lungs. It consists of a piston moving in a brass cylinder. The displacement of the pump (or tidal volume) is continuously variable between 400 and 3000 milliliters, and the cyclic rate (or respiratory rate) covers a range of 15 to 60 cycles/minute.

Determination of the oscillating flow velocities and flow volumes is accomplished as follows. Pressure drops, at some restriction within the flow path, are plotted using a pressure transducer. These pressure readings are then calibrated with a water manometer across the same restriction. A constant vacuum is used at this time in place of the lung simulating pump, since the response time of the manometer is much too slow to measure the cyclic flow. The vacuum is then adjusted to

*SC-TM-67-2962, Correlation of Surface Air Plutonium Concentrations with Measured Plutonium Lung Dose Content, R. J. Everett and W. D. Burnett, Sandia Laboratory, Albuquerque, New Mexico, November 1967.

CONFIDENTIAL

give differential pressure readings in the same range as those found using the pump. A rotometer in series with the flow is used to measure the flow rate in liters per minute. Assuming that no changes have taken place within the circuit, equal pressure points taken under static and dynamic conditions can be referenced to equal volume flow rates.

Figure 17 shows typical traces taken from the pressure transducer. The top curve was obtained using a human subject at rest, breathing about 15 times per minute, with a tidal volume of about 600 cubic centimeters. This is typical of breathing patterns reported in the medical literature. Exhalation (lower part of curve) takes place over a longer period of time than does inspiration and is followed by a brief pause.

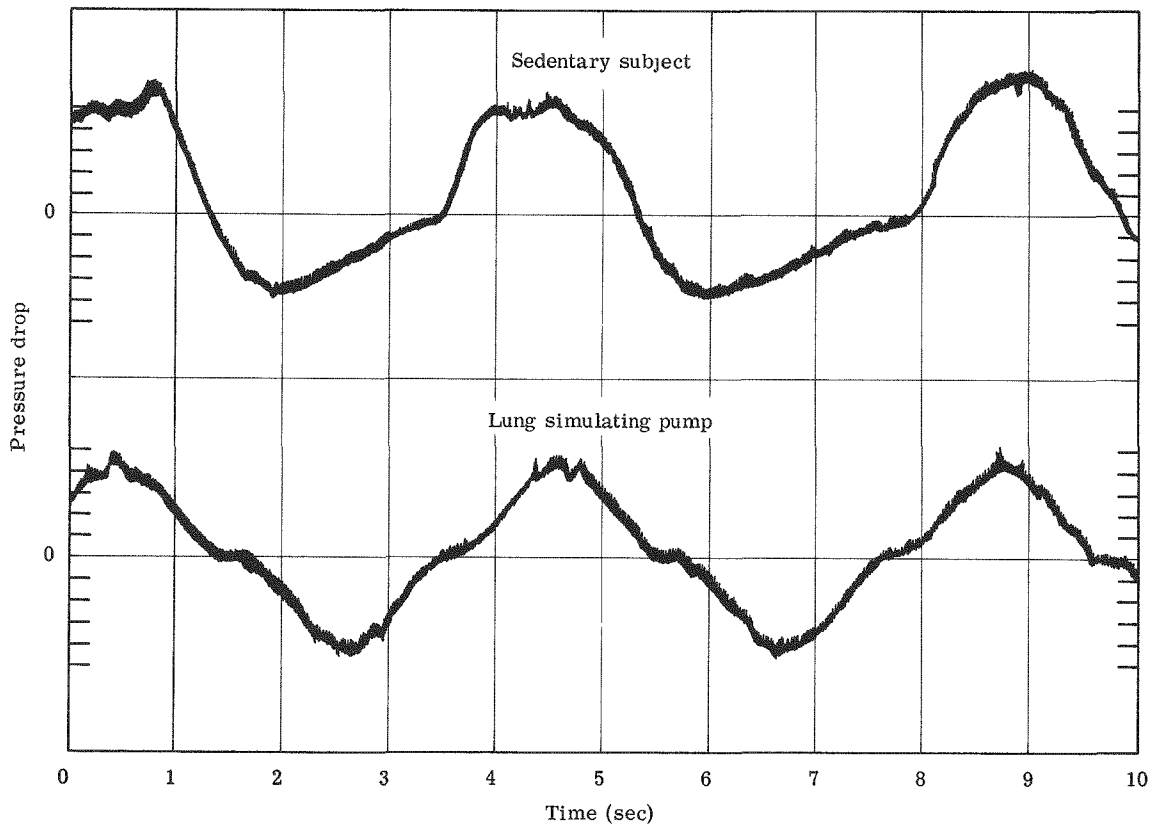



Figure 17. Data taken with fast-response differential pressure transducer (D68-11044)



The lung simulating pump (shown in lower part of Figure 17) was adjusted to give approximately the same cyclic rate as for the human and with the same peak pressure drop. Both flow circuits were through the same orifice and across a slight restriction. In the lower curve, however, the volume is only about 450 cm³. Preliminary trials, under steady flow conditions, using iron spheres have shown that no spheres larger than ~200 microns in diameter could be "inhaled" into a glass tube inverted at an angle of 60 degrees. These tests were run under maximum intake velocities for sedentary subjects (estimated at 370 cm/sec).

Polonium-Fueled Systems


SNAP-29

Polonium-210 in Soil (M. A. Parsont)

A contract review was made at Colorado State University, Department of Radiology and Radiation Biology, regarding DBM-sponsored research on the metabolism of ²¹⁰Po. Work is in progress to determine the distribution coefficients of ²¹⁰Po in soils, the effect of chemical composition on soil ion exchange properties, and root uptake of ²¹⁰Po by various plants. This review was conducted to maintain liaison for application to radiation risk assessment for SNAP-29.

Force and Moment Tests (D. E. Randall)

Static force and moment tests and aeroheating tests of two fuel block configurations (aspect ratios 1.74 and 3.2) were completed in AEDC Tunnel B (Mach 8). A new aerothermal test plan for the SNAP-29 fuel block was jointly arrived at by Martin and Sandia. This plan will increase the test time requirements by 24 hours over the previous test plan.



Escape of Polonium from a Punctured Capsule (D. C. Williams)

The results of the polonium release experiment performed at Mound Laboratory during July 1967 (designated "Air Exposure Test No. 2") were analyzed at Sandia. In the Mound experiment, a polonium fuel form (GdPo in a matrix) was placed in a capsule that was intentionally flawed with a pinhole (~6.8 mils diameter) and heated in air to 865°C. During the next 42 hours, massive release (~45 percent of the total) of polonium occurred.

The Sandia analysis shows that the gross features of the release of the polonium are consistent with a simple diffusion model. The basic assumptions are that the polonium is initially present as a nonvolatile compound, and it can escape from the capsule only insofar as air diffuses in through the small hole, oxidizes the polonium compound to a volatile form, and the vapor then diffuses out. It was found that this mechanism alone is sufficient to account for the most rapid rate of release that was observed; there is no need to postulate the existence of additional factors that would enhance the release.

There are factors which complicate the above interpretation, especially the fact that the orifice diameter increased tenfold during the experiment. This fact implies that the effective volatility of the polonium remaining in the capsule at the end of the experiment was considerably less than the volatility of Po metal. The lack of data as to the time period over which the enlargement occurred cloud the interpretation of the earlier stages of polonium release; however, a simple experiment (performed by Mound) showed that the stainless-steel end cap of the outer capsule would not corrode significantly in air alone at this temperature. Hence, the initial rapid release must have occurred with the orifice at essentially its original size.



Promethium-Fueled Systems

ADVANCED MANNED STRATEGIC AIRCRAFT (AMSA)

AMSA Capsule Impact Tests (W. J. Dalby)

A three-phase program was conducted to evaluate the impact resistance of the fuel capsule for the AMSA application. The fuel capsule may reasonably be expected to provide fuel containment under all except the most adverse conditions. Impacting the bare capsule at 185 to 200 percent of the experimentally determined sea level equilibrium velocity of approximately 340 ft/sec into soil and concrete targets did not appear to significantly impair the fuel containment capability of the capsule. Impacting the bare capsule into a rigid target (granite) at velocities as low as 85 percent of the sea level equilibrium velocity of 340 ft/sec, with the cylindrical axis of the capsule at 35 to 55 degrees with the normal to the target face, ruptured the capsule. All impact tests were performed with capsule heated to 300°F. A report describing these tests was published.*

*SC-DR-67-718, AMSA Fuel Capsule Impact Tests, W. J. Dalby, Sandia Laboratory, Albuquerque, New Mexico, August 1967.

~~CONFIDENTIAL~~

ADVANCED TECHNOLOGY

Basic Studies

HIGH TEMPERATURE CHEMISTRY (R. T. Meyer/H. S. Levine)

Previous conclusions* were reexamined regarding: (1) the sensitivity of the time resolved mass spectrometer for Langmuir vaporization studies, (2) the magnitude of radiation, conduction, and vaporization heat losses for pulse-heated metal samples, and (3) the significance of a 100°C discrepancy in the measured temperature for the α to β phase transition of Zr. The results now indicate that: (1) the sensitivity is equivalent to a partial pressure of 1×10^{-6} torr at 2000°K, (2) heat losses during 1 msec are indeed negligible, and (3) either the literature values for the specific heat and resistivity of Zr are in error or superheating of α -Zr occurs.

Further analysis of the diffusion of N_2 and O_2 through the walls of zirconia sacs indicated that the diffusion of both gases is equivalent and coupled. This means that the presence of either N_2 or O_2 at some finite pressure within the sac will prevent diffusion inward of N_2 and O_2 from the reactant environment during the transient period for zirconium combustion. Furthermore, if the sac is initially void of gas, N_2 and O_2 will diffuse inward in proportion to their external concentrations. The amount of N_2 which can diffuse from the threshold atmosphere for sac formation is significantly less than that detected mass spectrometrically.

OXIDATION OF ZIRCONIUM DROPLETS (L. S. Nelson)

The combustion of single droplets of zirconium in oxygen-containing atmospheres is being studied collaboratively with AeroChem Research Laboratories, Inc., Princeton, New Jersey. The joint program involves an

*SC-RR-67-760, Application of Time Resolved Mass Spectrometry to Problems in High Temperature Chemistry, R. T. Meyer and H. S. Levine, Sandia Laboratory, Albuquerque, New Mexico, August 1967.

~~CONFIDENTIAL~~

[REDACTED]

analytical effort to set up a model that describes the temperature and reaction rate histories of the oxidizing droplets and which is consistent with earlier experimental work performed at Sandia. The theoretical predictions are being used to devise new experiments for a test of overall consistency.

The model considers four regimes as follows, listed in order of increasing time of combustion:

1. Chemically controlled droplet heat-up to temperatures at which appreciable evaporation of zirconium-containing species can occur.
2. External transport/kinetic-controlled oxygen incorporation at nearly constant rate--unsaturated surface.
3. A cool-off period accompanying reduction in oxygen uptake rate due to surface saturation. Oxygen diffusion within the droplet governs the rate of O_2 -uptake and heat generation.
4. "Spearpointing" (recalescence) due to superficial (partial) solidification below the equilibrium freezing temperature followed by further cooling during the completion of solidification.

The new experimental program examines the combustion of zirconium droplets with both larger and smaller diameters than in previous work. The reactive environments of interest are oxygen at various total pressures and oxygen-argon and (new) oxygen-helium mixtures, with various partial pressures of oxygen and the diluent gas. Recording is done both photographically and with one or more photomultipliers equipped with narrow band filters. Electron microprobe scans of quenched and sectioned droplets are being made to determine, if possible, oxygen diffusion profiles at various combustion times.

The luminosity-time traces obtained from the photomultipliers provide valuable information about the oxidation. A typical curve from a Dumont 6911 photomultiplier filtered at 0.8 micron is shown in Figure 18 for a 525-micron-diameter droplet of zirconium burning in pure oxygen at 625 torr. The four regimes used in the model are thought to coincide with the portions of the trace marked 1 through 4. Notice the discontinuity at ~220 msec (the "spearpoint") that accompanies superficial solidification of the oxidized droplet after a period of supercooling.*

*L. S. Nelson, Nature, 207,741 (1965); 210, 410 (1966).

Traces similar to the one shown in Figure 18 provide the following parameters of importance in the combustion model:

t_{\max} , the time to maximum light intensity;

t_{sp} , the time to spearpoint;

t_{sol} , the time for initial solidification, i.e., rise-time of the spearpoint; and

$T(t)$, the apparent temperature as a function of time for the various droplet diameters and partial pressures of O_2 , Ar, and He.

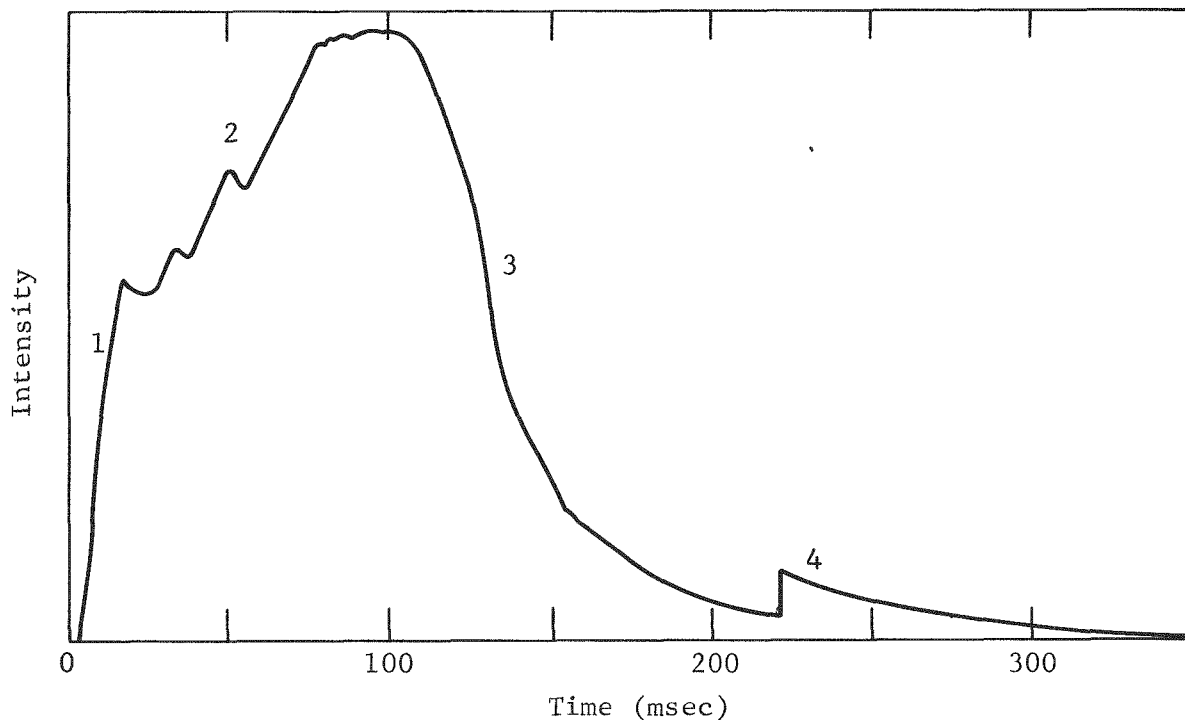


Figure 18. Luminosity-time trace for a $525\text{-}\mu$ Zr droplet burning in O_2 at 625 torr obtained from a Dumont 6911 photomultiplier filtered to record radiation at $0.8\ \mu$. Numbered portions of the trace are thought to correspond to the four regimes predicted by the AeroChem combustion model. (D68-11045)

Several trends are evident in the data. Both t_{\max} and t_{sp} increase as droplet diameter, and the ratios $p_{\text{Ar}}/p_{\text{O}_2}$ or $p_{\text{He}}/p_{\text{O}_2}$ increase. In pure O_2 , as p_{O_2} decreases for a given droplet diameter, both t_{\max}

~~CONFIDENTIAL~~

and t_{sp} are shorter in an O_2 -He mixture than in an O_2 -Ar mixture at the same total pressure and of the same percentage composition; and t_{sol} is less than 150 μ sec for a 525- μ droplet of zirconium burning in pure O_2 at 625 torr.

The photomultiplier records also offer considerable promise for high-speed pyrometry of incandescent droplets, both in oxidizing and in inert environments. Two approaches are being examined: (1) single-color brightness pyrometry referenced to the freezing temperature of the droplets at the "spearpoint," and (2) two-color ratio pyrometry referenced to a known blackbody source. Our apparatus permits both methods to be performed simultaneously, and the approaches should offer interesting cross-comparisons among the resultant temperatures. These data should provide important information about energy exchange between small particles and their surroundings at high temperatures (2000° to 5000°K).

INITIAL STAGES IN THE NITRIDATION OF METALS (R. A. Sallach)

Techniques were perfected for studying the initial stages of the reaction of nitrogen with active metals. By working at high temperatures and low gas pressures the duration of the initial stages was expanded to times greater than a minute.

Quantitative results were obtained for the reaction of nitrogen with zirconium at 1440°C, at pressures between 2×10^{-3} and 10×10^{-3} torr. An initial linear reaction regime is observed, followed by a transition to approximately parabolic kinetics. The duration of the linear regime is inversely proportional to the square of the pressure. From the linear rate of mass gain, it can be calculated that only 7 to 8 percent of the incident nitrogen gas flux to the metal surface reacts with the metal.

The experimental data can be fitted to a simplified theoretical reaction model from which a diffusion coefficient for N in β -Zr of 1.8×10^{-6} cm^2/sec can be computed; this is in good agreement with a published value. However, metallographic analysis indicates that the

~~CONFIDENTIAL~~

overall reaction is more complex, and the above value of the diffusion coefficient may be too large by as much as a factor of 2.

ATMOSPHERIC DISPERSION STUDIES

Stardust Atmospheric Fallout Diagnostic Studies (R. E. Smith)

The existing Stardust atmospheric fallout model (previously developed for NASA and AEC for the atmospheric weapons testing program by Isotopes, Inc.) is being used to determine the surface air and the ground concentrations of radionuclides accidentally injected into the stratosphere by a SNAP device. During the past quarter, a few minor modifications were made to the Stardust computer program by Isotopes, Inc., so that the model could be used for injections of slightly larger and heavier debris (up to 0.5 μ , density 10 g/cc) that may be more representative of SNAP debris injection instead of the small atomic weapon debris (<0.2 μ , density 2 g/cc) used in the previously developed model. The one apparently successful computer run received shows that for 0.5- μ particles injected at 20°N latitude during the winter season at an altitude of 375 km, 26 percent reached the ground at the end of 1 year. Based on this information, additional injections of similarly sized particles at several latitudes of injections for run periods of 2 years are currently being performed by Isotopes, Inc., for Sandia.

AUTOROTATION STUDIES (G. W. Stone)

The general investigation of the dynamics and aerodynamics of autorotating bodies has continued, and four significant milestones have been passed. In September, the second test of autorotating flat plates was conducted at the Edgewood Arsenal subsonic wind tunnel with a new support system and 13 flat plate configurations. The flat plate models included rectangular plates with aspect ratios from 1/6 to 6, thin circular disks, circular fuel puck configurations, triangular plates, and two SNAP-29 plates. This test was conducted at air velocities from 25 to 150 mph, and excellent dynamic data were obtained.

[REDACTED]

On October 2, the first hypersonic free-flight autorotation test was conducted on flat plates, disks, and cylinders at the AEDC Wind Tunnel B. Good quantitative data were obtained on many of the models; however, because of the short test time (0.2 second or less), very little data were obtained for the plates.

On November 17-18, the first one-degree-of-freedom hypersonic autorotation test was conducted on SNAP-19 capsule configurations in the Sandia 18-inch Hypersonic Wind Tunnel. The test was conducted at Mach numbers of 5, 7.3, and 11. The configurations tested were the basic cylinder and the cylinder with 0.15D, 0.30D, and 0.45D end cuts at 180-degree relative roll positions. Although there were minor problems with the test rig and procedure that will necessitate additional tests, valuable data were obtained for the SNAP-19 program. The cylinder with 0.45D end cuts achieved a 15,000 rpm angular rate during the test.

On November 27, the same four cylindrical configurations were tested subsonically at Edgewood Arsenal using a new support system for cylinders. Excellent dynamic data were obtained on the cylinders for air velocities from 25 to 190 mph. This was the first test that included studies on the effects of edge shape on autorotation.

FUEL PUCKS

CMA Computer Ablation Estimates (D. E. Randall)

The CMA computer program was used to estimate the ablation of two fuel puck configurations. The configurations analyzed were 1- and 5-inch diameter circular disks with thickness-to-diameter ratios of 1/20 and 1/10, respectively. The characteristic motion was assumed to be tumbling about a diametral axis. The smaller puck proved unsatisfactory in that the graphite protective shell ablated through shortly after the puck's release along a typical reentry trajectory. The graphite shell on the larger puck survived very nearly to impact, and fuel temperatures did not reach the melting point for the trajectories studied. The analysis indicates the desirability of tailoring the graphite shell thickness to the heating distribution around the puck.



CAPSULE IMPACT (W. J. Dalby)

A theoretical and experimental study of the effects of impact on spherical shells was conducted by the Engineering Experiment Station, Georgia Institute of Technology, Atlanta, Georgia, under Sandia contract.* The theoretical study is based upon the equations of equilibrium derived from the three-dimensional equations of elasticity within the limitations of the Kirchhoff assumptions, constitutive equations describing an isotropic material which satisfy a bilinear stress-strain displacement relation, and linear moment curvature equations. Spherical shells of 0.75- to 1.25-inch outside diameter and with 0.08- to 0.13-inch wall thickness were fabricated and impacted at 50 to 800 fps into steel targets with the shells at ambient temperature.

An earlier report describes theoretical study of the high-velocity impact of hollow cylindrical shells.** The cylindrical shell was treated as a membrane by a modified strain rate theory to approximate plastic wave propagation. An elastic bending theory was also investigated and was compared to the membrane theory. Radial deflections were investigated under various end conditions. A failure criterion was established, and theoretical and experimental failure velocities were compared. These efforts were also conducted by the Engineering Experiment Station, Georgia Institute of Technology, Atlanta, Georgia, under Sandia contract.

* SC-CR-67-2540, A Study of Impact Effects on Spherical Shells, Part 2, A Theoretical and Experimental Study of the Response of Spherical Shells to Impact Loads, Georgia Institute of Technology, Sandia Laboratory, Albuquerque, New Mexico, November 1967.

** SC-CR-67-2135, A Study of Impact Effects on Spherical Shells, Part 1, A Theoretical Study of the Response of Hollow Cylinders to Impact Loads, Georgia Institute of Technology, Sandia Laboratory, Albuquerque, New Mexico, October 1967.



CONFIDENTIAL

FUEL/CLAD/SOIL REACTION (J. B. Boyd)

The soils investigation report was received from the University of New Mexico and published.* Except for occasional consultant services related to soils investigations by Sandia, the UNM contract work is complete.

Work continues on the National Bureau of Standards contract to determine the effective thermal conductance of selected soils. All laboratory apparatus materials have been ordered. The cooling coils for the laboratory apparatus were built and tested. Initiation of soil conductivity measurements is planned in January 1968.

SOIL CONDUCTIVITY (F. L. Baker/P. L. Class)

The HERMAN heat transfer program is being used in an effort to determine an effective thermal conductance for the soils used in the SNAP-27 burial test program. The method in use approximates the SNAP-27 experimental data (temperature versus time) by changes to the program conductivity input in successive computer runs. The initial conductivity values were obtained by extrapolating available data to the higher temperatures experienced in the tests. The preliminary information presented in Figures 19 through 21 illustrates the progress made to date.

GENERAL STUDIES

Publication of SC-RR-67-232 (R. D. Klett)

SC-RR-67-232, Reentry Temperatures of Low Heat Capacity Structures, by R. D. Klett, was published by Sandia. Equations were derived for computing the temperatures of low heat capacity structures during reentry for free molecule and continuum flow. These equations were solved for altitudes from 0 to 700,000 feet, velocities from 6000 to 38,000 fps, initial temperatures from 500° to 1500°R, and for all expected values of dimensionless groups, which include thermal emissivities and heating ratios. The results are presented in graphical form. The uses and limitations of these graphs for analyzing reentering structures are discussed.

*SC-CR-67-2688, The Fusion of Soils, University of New Mexico, Sandia Laboratory, Albuquerque, New Mexico, November 1967.

CONFIDENTIAL

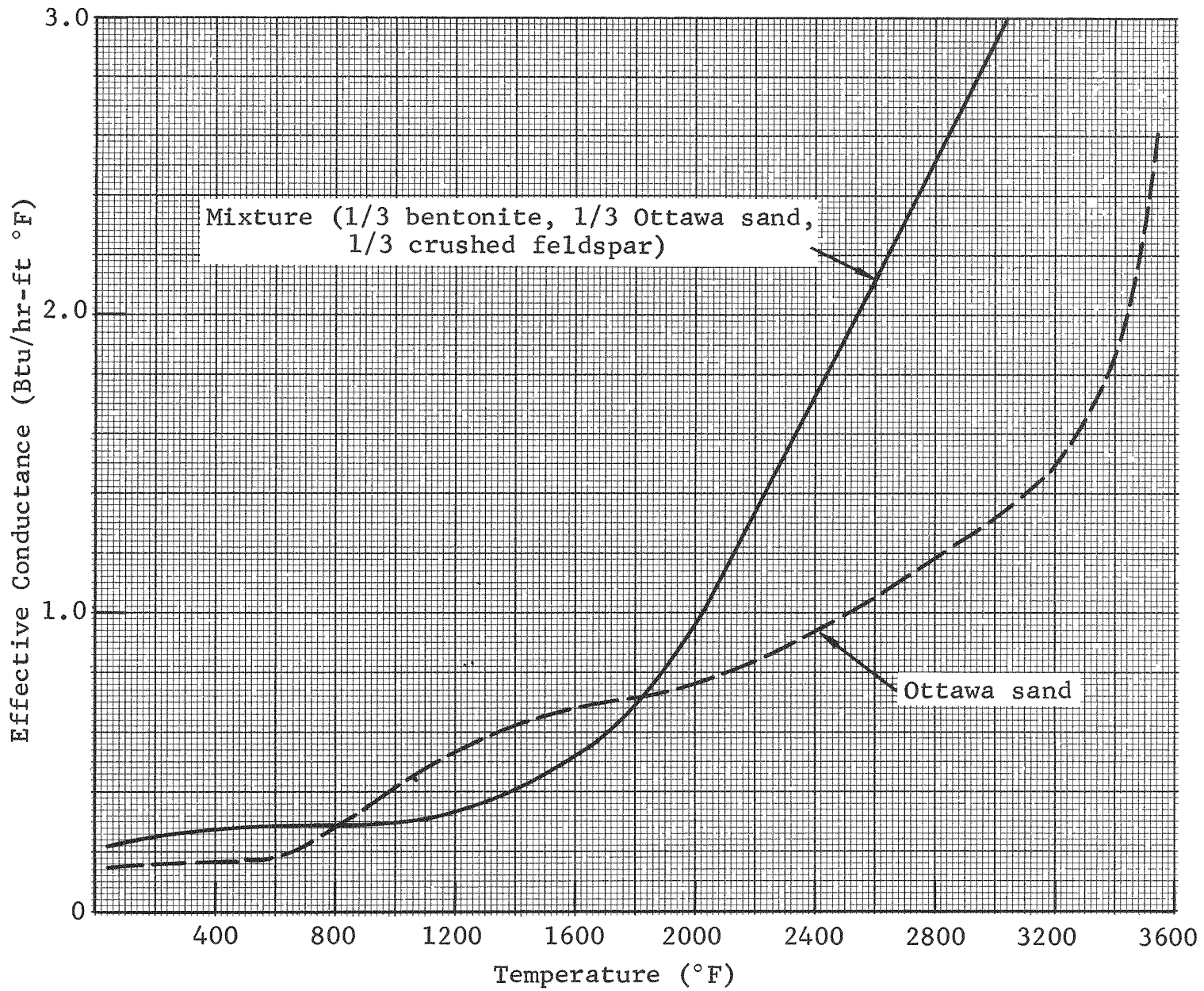


Figure 19. Effective thermal conductance versus temperature for Ottawa sand and the mixture (D68-11046)

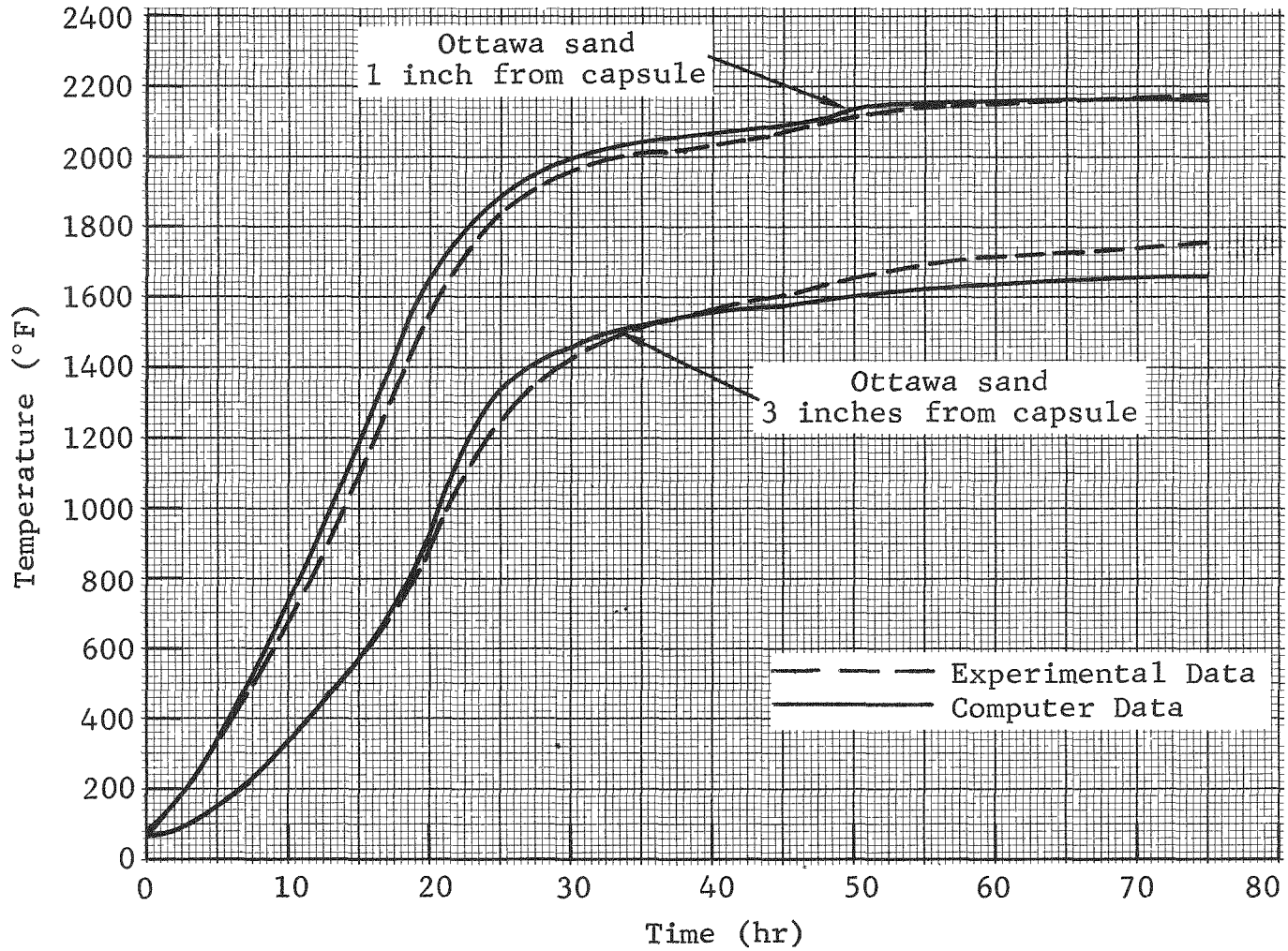


Figure 20. Experimental and computer data for Ottawa sand (D68-11047)

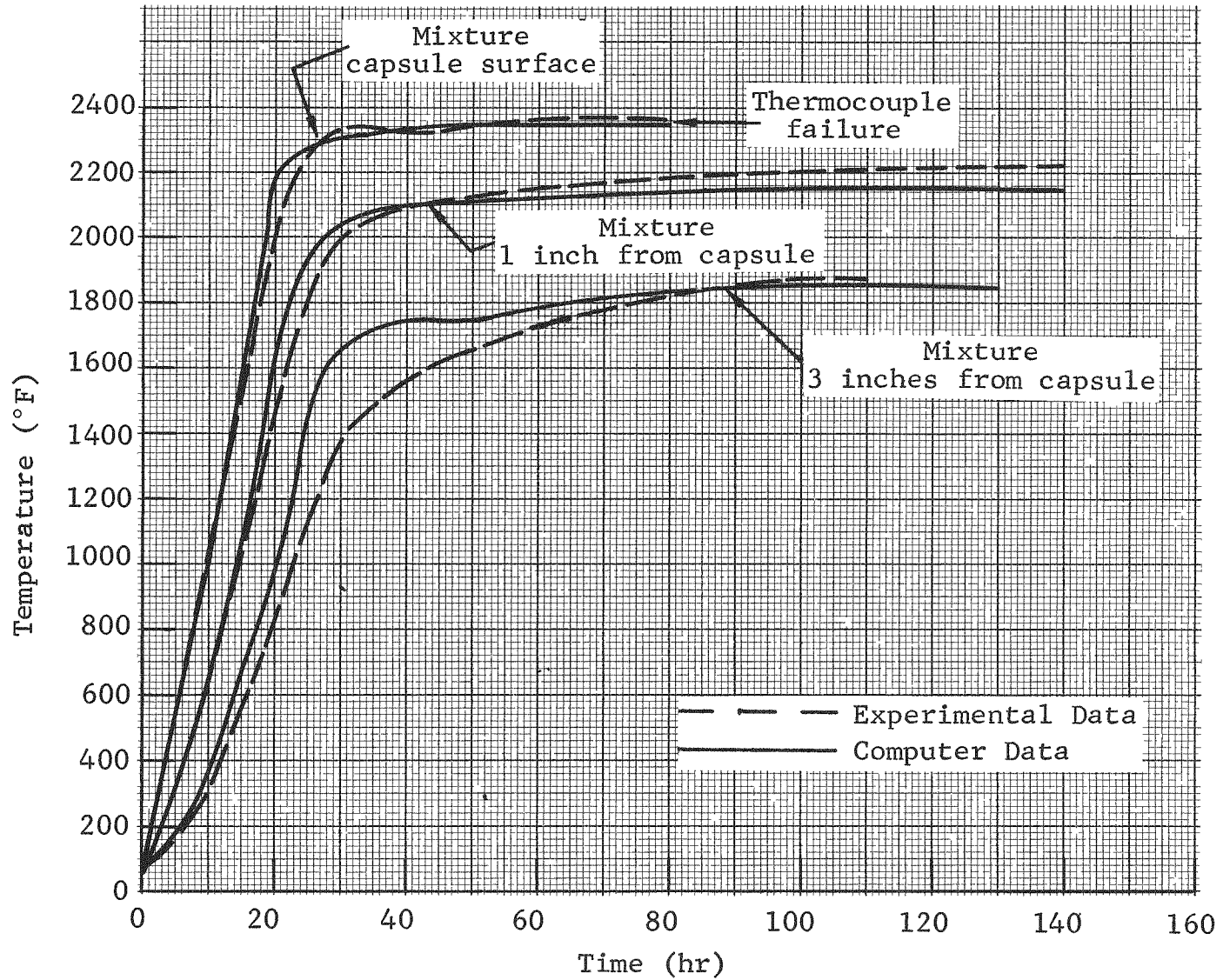


Figure 21. Experimental and computer data for the mixture (D68-11048)

~~CONFIDENTIAL~~

DEMOGRAPHIC STUDIES (E. S. Phinney)

A population data tape programmed for the IBM 360 was prepared and transmitted to Atomics International for their use in support of the soils study they are doing for the Sandia ANS Department. A copy of this tape was also sent to Martin-Marietta for their use in the safety study of the SNAP-29. An additional copy of this tape was sent to the National Military Command System Support Center for their information and possible utilization. An identical tape programmed for the CDC 3600 was sent to NASA Headquarters for their use in evaluation of their contractor's population analyses. These tapes contain almost complete world population data, with the exception of some small islands.

COMPUTER CODES (H. R. Spahr)

Computer Code HRS004

This computer code calculates the initial velocity and reentry angle for objects decaying from circular earth orbits. Version 7 of this code is now operational on the Sandia Quicktran remote terminal. Use of this terminal with the IBM 7040/44 computer in Los Angeles provides results in 15 minutes rather than the 4 to 8 hours required previously. Reports describing the theory used in HRS004 and versions 1 through 6 of it are in preparation.

Martin FB-123 Computer Code

The source deck, binary deck, sample input, sample output, and documentation were received for the Martin FB-123 computer code. This code computes the Newtonian aerodynamic coefficients for a shape and prepares a tape for a plotter to draw the configuration at the specified angle of attack.

New Computer Codes

The following computer codes were written for the analysis of heating rates near the titanium struts on the GLFC:

~~CONFIDENTIAL~~

~~CONFIDENTIAL~~

- HRS009 - Computes the conditions upstream and downstream of a normal shock, after an isentropic expansion from stagnation conditions.
- HRS010 - Computes stagnation point reference heating rate, DQC, given air density and velocity.
- HRS011 - Computes air viscosity given enthalpy and pressure.
- HRS013 - Computes heating rate to a surface for a laminar boundary layer.

These codes are operational on the IBM 7040/44 in Los Angeles, via the Sandia Quicktran remote terminal.

AEC MEETING ON SEARCH, DETECTION, AND RECOVERY OF RADIOISOTOPE HEAT SOURCES (R. C. Cranfill)

The AEC Space Nuclear Systems Division will sponsor a meeting on the subject of search, detection, and recovery of radioisotope heat sources. Sandia Laboratory will host and assist in planning the meeting which will be held January 16 through 18, 1968. The primary intent of the meeting is to provide information on present and projected capabilities relative to tracking, search, detection, recovery, and/or decontamination following potential preorbit or orbital aborts during typical SNAP missions. From a safety point of view, recovery of the radioisotope fuel (or firm knowledge that deep ocean disposal of the radioisotope fuel was accomplished) in the event of an abort is extremely desirable.

Administrative

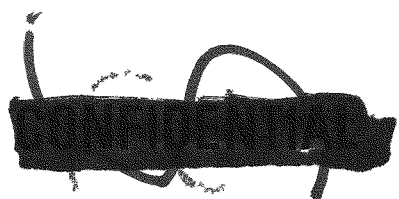
ESTABLISHMENT OF NEW STANDARD ANS DOCUMENT DISTRIBUTION (R. G. Illing)

Sandia ANS document distribution was established through the AEC Division of Technical Information Exchange (DTIE) at Oak Ridge. As the culmination of a number of months of effort, DTIE substantially revised the unclassified UC-36 and classified C-44d standard ANS distribution

~~CONFIDENTIAL~~



lists. Use of the standard distribution is expected to substantially reduce the administrative and mail channel problems previously experienced by Sandia when we directly controlled the report distribution. Bulk quantities of ANS reports will now be sent to DTIE for standard distribution. A limited supplementary distribution will be made directly by Sandia to key agencies requiring immediate access to the information.



[REDACTED]

SPECIFIED EXTERNAL DISTRIBUTION ONLY

DISTRIBUTION:

M-3679 (53rd Ed.) C-44d (120)

U. S. Atomic Energy Commission
Division of Space Nuclear Systems
Space Electric Power Office
Washington, D. C. 20545

Attn: G. A. Newby,
Assistant Director (1)
G. P. Dix, Chief
Safety Branch (1)
R. S. Decker, Chief
Safety Branch (1)
R. T. Carpenter, Chief
Isotope Power Br. (1)
J. A. Powers, Chief
Isotope and Matls. Br. (1)
C. E. Johnson, Chief
Reactor Power Sys. Br. (1)
Division of Isotope Development (1)
Division of Biology and Medicine
Attn: J. Z. Holland, Chief
Fallout Studies Br. (1)
H. D. Bruner, Asst. Med.
and Health Research (1)
Office of Director of Regulation
Attn: C. K. Beck
Deputy Director (1)
F. D. Anderson, Regulation (1)

U. S. Atomic Energy Commission
Albuquerque Operations Office
P.O. Box 5400
Albuquerque, New Mexico 87115
Attn: Space Nuclear Propulsion
Office, Albuq. Extension
For: S. A. Upson, Director
Nonnuclear Activities Div.
G. H. Dugger, Acting Director
Operational Safety Division

AEC Site Representative
National Aeronautics and Space Adm.
Manned Space Center
Houston, Texas 77058
Attn: W. C. Remini
Bldg. 16, Code ZS-5

Deputy I. G. for Insp. & Safety
USAF
Kirtland Air Force Base
New Mexico 87117
Attn: Col. D. C. Jameson (AFINSR)

Los Alamos Scientific Laboratory
P.O. Box 1663
Los Alamos, New Mexico 87544
Attn: Dr. L. D. P. King (1)
Dr. Wright Langham (1)
C. F. Metz, CMB-1 (1)
F. W. Schonfeld, CMF-5 (1)

Martin-Marietta Corporation
Martin Company
Nuclear Programs
Middle River, Maryland 21203
Attn: D. Anderson

Monsanto Research Corporation
Mound Laboratory
P.O. Box 32
Miamisburg, Ohio 45342
Attn: G. R. Grove

Thomas B. Kerr
Code RNS
National Aeronautics and Space Adm.
Washington, D. C. 20546

National Aeronautics and Space Adm.
Goddard Space Flight Center
Glenn Dale Road
Greenbelt, Maryland 20771
Attn: A. W. Fihelly,
Nimbus Project

Space Nuclear Propulsion Office
Lewis Research Center
21000 Brookpark Road
Cleveland, Ohio 44135
Attn: L. Nichols

TRW Systems
P.O. Box 287
Redondo Beach, California 90278
Attn: Dr. Donald Jortner

J. R. Banister, 5120
J. D. Shreve, 5234
D. B. Shuster, 5600
H. E. Viney, 7130
L. E. Lamkin, 7300
G. A. Fowler, 9000
A. Y. Pope, 9300
Attn: V. E. Blake, 9310
H. E. Hansen, 9311

~~CONFIDENTIAL~~

DISTRIBUTION (cont):

- S. L. Jeffers, 9312
- S. McAlees, Jr., 9314
- R. J. Everett, 9315
- J. D. Appel, 9319
- J. D. Appel, 9319 (ANSIC) (2)
- R. C. Maydew, 9320
- A. J. Clark, 9330
- J. W. McKiernan, 9331
- R. P. Stromberg, 9333
- B. F. Hefley, 8232
- B. R. Allen, 3421
- L. C. Baldwin, 3412
- L. L. Alpaugh, 3412
- C. H. Sproul, 3428-2 (10)

~~CONFIDENTIAL~~